Bioactive Materials 26 (2023) 142–158

Contents lists available at ScienceDirect

Bioactive Materials

journal homepage: www.keaipublishing.com/en/journals/bioactive-materials

Hydrophobic aerogel-modified hemostatic gauze with thermal management performance

Xiaoli Jia [a,b,f,1], Chao Hua [a,c,1], Fengbo Yang [a,b,1], Xiaoxiao Li [d], Peng Zhao [a], Feifan Zhou [c], Yichi Lu [b], Hao Liang [e], Malcolm Xing [f,*], Guozhong Lyu [a,b,c,d,**]

[a] Engineering Research Center of the Ministry of Education for Wound Repair Technology, Jiangnan University, Affiliated Hospital of Jiangnan University, Wuxi, 214000, China
[b] Wuxi School of Medicine, Jiangnan University, Wuxi, 214000, China
[c] Medical School of Nantong University, Nantong, 226019, China
[d] Nanjing University of Traditional Chinese Medicine, Nanjing, 210023, China
[e] Changhai Clinical Research Unit, Shanghai Changhai Hospital, Naval Medical University, Shanghai, 200433, China
[f] Department of Mechanical Engineering, University of Manitoba, Winnipeg, R3T 2N2, Canada

ARTICLE INFO

Keywords:
Hydrophobic hemostasis
Thermal management
Hydrophobic methyl modified nano-silica aerogel
Harsh environments
Unidirectional fluid pumping

ABSTRACT

Current hemostatic agents or dressings are not efficient under extremely hot and cold environments due to deterioration of active ingredients, water evaporation and ice crystal growth. To address these challenges, we engineered a biocompatible hemostatic system with thermoregulatory properties for harsh conditions by combining the asymmetric wetting nano-silica aerogel coated-gauze (AWNSA@G) with a layer-by-layer (LBL) structure. Our AWNSA@G was a dressing with a tunable wettability prepared by spraying the hydrophobic nano-silica aerogel onto the gauze from different distances. The hemostatic time and blood loss of the AWNSA@G were 5.1 and 6.9 times lower than normal gauze in rat's injured femoral artery model. Moreover, the modified gauze was torn off after hemostasis without rebleeding, approximately 23.8 times of peak peeling force lower than normal gauze. For the LBL structure, consisting of the nano-silica aerogel layer and a *n*-octadecane phase change material layer, in both hot (70 °C) and cold (−27 °C) environments, exhibited dual-functional thermal management and maintained a stable internal temperature. We further verified our composite presented superior blood coagulation effect in extreme environments due to the LBL structure, the pro-coagulant properties of nano-silica aerogel and unidirectional fluid pumping of AWNSA@G. Our work, therefore, shows great hemostasis potential under normal and extreme temperature environments.

1. Introduction

Uncontrolled hemorrhage is a major obstacle for medical treatment. When vascular damage occurs, platelets and coagulation factors in the blood work together to form a coagulation to prevent bleeding. However, in harsh hot and cold environments, extremely cold stress may impair the function of platelets and off-chart hot stress may weaken the activity of coagulation factors. All these increase blood flow rates and activate the fibrinolytic system and ultimately make hemostasis more challenging [1–4]. Blood is essential for transporting oxygen and nutrients to the body's tissues and organs, and it is vital for excreting metabolic waste products [5]. In addition, blood maintains the systemic homeostasis by absorbing and distributing heat throughout the body [6]. Excessive blood loss can cause a range of complications such as hypothermia, coagulation disorders, perfusion deficit and shock [7,8], leading to 15–25% of trauma deaths and over 50% of battlefield casualties during the prehospital stage [9,10]. Therefore, it is significant for the wounded to have emergent and efficient measures to control bleeding. However, existing hemostatic agents or dressings have been associated with poor hemostatic performance in hot/cold conditions,

Peer review under responsibility of KeAi Communications Co., Ltd.
* Corresponding author.
** Corresponding author. Engineering Research Center of the Ministry of Education for Wound Repair Technology, Jiangnan University, Affiliated Hospital of Jiangnan University, Wuxi, 214000, China.
E-mail addresses: malcolm.xing@umanitoba.ca (M. Xing), Luguozhong@jiangnan.edu.cn (G. Lyu).
[1] These authors contributed equally to this manuscript.

https://doi.org/10.1016/j.bioactmat.2023.02.017
Received 31 October 2022; Received in revised form 13 February 2023; Accepted 14 February 2023

due to their lack of thermal management properties.

Mechanically pressing the wound with cotton gauze is a conventional hemostatic measure [11]. However, in ultra-cold conditions, the blood in the gauze forms ice crystals that can damage wound repair cells and eventually adversely affect the patient's prognosis [12,13]. Sealants or glues such as fibrin, chitosan and modified sodium alginate serve as efficient hemostatic agents by sealing arterial and tissue defects [14–16]. Nevertheless, these water-rich hydrogels show the fast evaporation of water at severe high temperature and the accelerated formation of ice crystals internally at severe low temperature, and thus become ineffective in harsh environment [17–19]. Thrombin and fibrinogen are essential in the intrinsic and extrinsic coagulation pathways, and their concentrations can greatly influence the stability and structure of blood clots [20,21]. Several materials have been approved by US Food and Drug Administration (FDA), such as Tissel®, Evicel® and Artiss®, achieve efficient and rapid hemostasis, mainly due to their high levels of thrombin and fibrinogen content [20,22]. However, due to the denaturation of proteins at high temperatures [23,24], the functions of fibrinogen and thrombin are degraded and therefore not applicable for hemorrhage control in extremely thermal environments. Biomimetic mineralized thrombin can maintain a high level of enzymatic activity in extremely hot conditions at 70 °C [25]. The loading on dopamine-treated gauze prevents its washing away by massive bleeding and enables rapid hemostasis [25]. But the blood absorbing in the hydrophilic cotton gauze develops a strong gauze-clot complex, the removal of which often cause pain or even secondary bleeding [26]. Given the limitations of the aforementioned materials, there is a desperate need to develop novel and easily removed hemostatic materials with temperature regulation capabilities for application in harsh hot/cold environments.

Herein, we aim to design and fabricate a highly effective and easy peeling hemostatic material with thermal management performance that can protect the wound microenvironment from extremely hot or cold stress in the external surroundings. Due to the low thermal conductivity and density, silica aerogels are superior choice for thermal management [27,28]. They can keep cool in harsh hot environments by blocking out heat conduction and keep warm in harsh cold environments by reducing energy loss [29]. However, aerogels are passive barrier materials for insulating temperatures and they lack smart energy management. Phase change materials (PCMs) are materials with phase transformations that occur with temperature fluctuations by absorbing heat or releasing latent energy [30,31]. Recently, a layer-by-layer (LBL) structure, combined with a hydrophobic silica aerogel layer as exposed to the outer surrounding and a PCM layer as inner layer, has been proposed, showing efficient thermal management capabilities [32], but the research in hemostasis, especially under harsh environments, has not yet been reported. Zeolite and molecular brush materials, which are mainly composed of silica, have demonstrated excellent hemostatic properties through their characteristics of high porosity and specific surface area, indicating the hemostatic potential of hydrophobic silica aerogel [33,34].

In this work, it was hypothesized that hydrophobic methyl (CH_3-) tailored nano-silica aerogel with thermoregulatory properties can be an efficient and easily removed hemostatic agent. Under this consideration, we prepared a hemostatic composite material applicable to harsh environment by spraying hydrophobic nano-silica aerogel onto gauze and combining it with a LBL structure (Scheme). We first verified the efficient hemostatic performance of the hydrophobic nano-silica aerogel-coated gauze *in vitro and in vivo* and then demonstrated the easy peeling behavior of the modified gauze. Subsequently, we examined the dual thermal management properties of the LBL structure, Finally, the *in vitro* coagulation and hemostasis mechanism of the composite system, containing the LBL structure and hydrophobic nano-silica aerogel-coated gauze, was investigated in extreme environments.

2. Materials and methods

2.1. Materials

Cotton gauze was bought from the commercial market in China. Sodium silicate was obtained from Shanghai Macklin Biochemical. Co., Ltd, China. Hexamethyldisilylamine (HMDS) and hexamethyldisiloxane (HMDSO) were purchased from Aladdin Biochemical. Co., Ltd, China. Phase change microcapsules (MicroDelivery thermoregulation microcapsule) were obtained from Anhui Micro Delivery Smart Microcapsule Sci & Tech Co. Ltd., China. Acetone and Sulfuric acid (98 wt %) were provided by Sinopharm Chemical Reagent Co., Ltd., Shanghai, China. Calcein/PI Cell Viability/Cytotoxicity Assay Kit and lactate dehydrogenase (LDH) Release Assay Kit were provided from Beyotime Biological Reagent Co. Ltd, Shanghai, China. CCK8 Assay kit was bought from MedChemExpresss LLC, Shanghai, China. Rat active coagulation factor XII (FXIIa) was bought from Hengyuan Biotech Co. Ltd, Shanghai, China. Rat prothrombin fragment 1 + 2 (F1+2) ELISA Kit was purchase from provided by Cusabio Biotech Co. Ltd, Shanghai, China. The digital push & pull tester was purchased from Yueqing Handpi Instruments Co., Ltd, China. Male Sprague–Dawley (SD) rats (6–7 weeks old) were obtained from Changzhou Cavens' Lab Animal Co., Ltd, China. L929 cells (Cat. No. CCL-1) were acquired from ATCC.

2.2. Fabrication of the hemostatic composite with thermal management properties

Engineering of the composite hemostatic dressing with thermal management performance has many steps, including synthesis of hydrophobic nano-silica aerogel, coating hydrophobic nano-silica aerogel onto gauze, and fabrication of LBL structure.

2.2.1. Synthesis of hydrophobic nano-silica aerogel

Hydrophobic nano-silica aerogel was synthesized by a simplified solvent-boiling process using sodium silicate as a precursor [32]. In detail, 17 g of sodium silicate was dissolved in 34.3 ml of distilled water to form a homogeneous solution. Then, the solution was slowly added into stirred 24.8 ml of 40% sulfuric acid, and 10 M NaOH was applied dropwise to adjust the pH. Allowing the precursor solution to stand for 10 min after the pH value reached 5 to form a hydrogel. The gel was aged at 50 °C for 5 h, then crushed and mixed with HMDSO and HMDS, and stirred in an 80 °C of water bath. After 30 min, white solids were observed to form and float on the surface of the mixed liquid system. The white solids were subsequently rinsed and atmospherically dried to acquire nano-silica aerogel.

2.2.2. Preparation of cotton gauze coated with hydrophobic nano-silica aerogel

0.5 g of nano-silica aerogel was added to 30 ml of acetone and sonicated for 40 min to form the dispersion. Then the homogeneous dispersion was sprayed onto the gauze surface by using a spray gun and dried at 60 °C for 2 h. The spraying pressure was 2 MPa. The spraying distance between the nozzle of spray gun and cotton gauze was varied from 2 to 15 cm. To remove any loosely attached silica aerogel, the gauze was exposed to compressed gas from the spray gun, washed in distilled water and dried at 60 °C. The amount per unit area (APUA) of nano-silica aerogel on gauze (mg/cm^2) was calculated using the formula:

$$\text{APUA of nano-silica aerogel on gauze} = (W_n - W_o)/ S$$

where W_o, W_n, and S mean original gauze weight before nano-silica aerogel spraying, gauze weight after nano-silica aerogel spraying, and surface area of gauze.

2.2.3. Fabrication of a layer-by-layer (LBL) structure and its temperature insulation performance test

The LBL structure consisted of a nano-silica aerogel layer and a PCM layer, where the nano-aerogel layer was in touch with the heating/cooling plate and the PCM was the inner layer. The thicknesses of the nano-silica aerogel and PCM layers were 3 mm. A thermal camera (Haikang, China) was used to monitor the temperature. We recorded the temperatures at 5 points on the diameter of the circular sample and calculated the average value (Fig. 10b).

2.3. Physicochemical characterizations of the hydrophobic nano-silica aerogel and modified gauze

2.3.1. Structural characterization

The water contact angles (WCAs) were determined by a contact angle meter (Powereach JC2000D1). The FTIR spectrum was recorded by a Nicolet iN10 spectrometer. Size distribution was determined by a Malvern size analyzer. The surface structure and elemental components were observed by a scanning electron microscope (SEM) apparatus (Hitachi Co., Ltd.) equipped with an analytical assembly for detecting energy dispersive spectroscopy (EDS). The structural morphologies of nano-silica aerogel were got by a transmission electron microscope apparatus (TEM, Hitachi JEM-2100). The porous structure and specific surface area (SSA) of the nano-aerogel were detected by the standard Brunauer−Emmett−Teller (BET) approach, working on the basis of N_2 adsorption at pressures of $0.05 < P/P_0 < 0.3$.

2.3.2. Water vapor transmission and water uptake of gauze

To test water vapor permeation, a Teflon tube filled with 10 ml of deionised water was covered with our gauzes. Sealing the circumferential border firmly to avoid any penetration of water vapor through it. After placed at 37 °C for 24 h, the water vapor transmission rate (WVTR) was measured by weighing the mass loss of water in the Teflon tube. The WVTR (g/m^2/day) was calculated according to the formula:

$$WVTR = (M_b - M_a)/ A$$

where M_b, M_a, and A mean the Teflon tube mass before evaporation of water, the Teflon tube mass after evaporation of water, and the area of the Teflon tube mouth (m^2).

To measure water uptake, gauze with a size of 1.5 cm × 1.5 cm was immersed in SBF, subsequently it was taken out and put on an absorbent paper to remove excess water at set time interval. The gauze weight before (W_b) and after (W_a) immersion in SBF was determined, and water uptake of gauze was calculated using the formula:

$$\text{Water uptake } (\%) = (W_a - W_b)/ W_b \times 100\%$$

2.3.3. Research on unidirectional fluid pumping effect of gauze in a simplified model

A syringe was positioned over the gauze and supplied with green fluorescence-tagged simulated body fluid (SBF) (1% sodium fluorescein) at a rate of 120 μ L/min via a micro syringe pump. To make the fluorescence-labelled SBF visualizable, the fluid transport action of the gauze was recorded under UV light exposure at 245 nm. The hydrophobic top layer of gauze was prepared by spraying hydrophobic nano-silica aerogel at 2 cm.

2.4. Biocompatibility of gauze

Hemocompatibility was analyzed by viewing and measuring the release of hemoglobin from erythrocytes [72]. Erythrocytes were acquired by centrifuging whole blood at 150 g for 15 min. Subsequently, erythrocytes were washed by PBS for three times and diluted to a 2% (v/v) concentration. Afterwards, erythrocytes suspension was pipette to a centrifuge tube in touch with the gauze at 37 °C. After 1 h of incubation, the mix was centrifuged. The OD of the supernatant at 540 nm was measured by a microplate reader.

Cell compatibility of the hydrophobic silica aerogel coated-gauze was assessed using two methods including CCK8 assay kit and Calcein/PI cell viability/cytotoxicity assay kit according to the manufacture's instruction (an extraction approach and direct exposure test between gauze and cells) [51,73]. Briefly, after sterilized by 75% alcohol and 245 nm UV light irradiation, the gauze was placed in the bottom of a 24-well cell culture plate. 1 ml of L929 cells suspension at a density of 8×10^4 cells/mL was seeded onto the gauze surface and cultivated in a humid incubator with 5% CO2 at 37 °C for 24, 48, and 72 h. Afterwards, remove the medium and wash the cells with PBS. 0.5 μL of Calcein-AM and 0.5 μL of PI was mixed into 250 μL of buffer and then co-incubated with the cells for 30 min. Lastly, live cells with green fluorescence and dead cells with red fluorescence were observed by an inverse fluorescent microscope. The fluorescence intensity was quantified with Image J. As for the CCK8 testing, 100 μL of L929 cells with a density of 2×10^4 cells/mL was gently seeded in a 96-well plastic culture plate. After 12 h, extracts of gauze were added in the wells and incubated with cells for 24, 48, and 72 h. Then, CCK8 regents were applied and cultured for 2 h, and the optical density (OD) of each well was determined at 450 nm. Calculating cell viability according to Eq.:

$$\text{Cell viability } (\%) = (ODa - ODb)/ (ODc - ODb) \times 100\%$$

where ODa is the optical density of well with L929 cells and gauze extracts, ODc is the optical density of well with L929 cells, and ODb is the optical density of well without L929 cells.

Skin compatibility was examined by contacting our material with rat skin for 12 h [26]. A rat was anesthetized and its back hair was removed. The sample preparation for skin compatibility assessment was depicted in Fig. 6e, with an 8 mm by 8 mm silica aerogel-coated gauze attached onto a 16 mm by 16 mm normal gauze. Then, the sample was applied to the skin of the rat's back with medical adhesive tape. After 12 h, the gauze was removed from the anesthetized rat and any differences between the skin areas under the silica aerogel-coated gauze and the normal gauze were observed.

2.5. Hemostasis evaluation in vitro

In vitro, hemostasis was evaluated by blood coagulation index (BCI) assay plasma clotting assay, detection kits and SEM observation.

2.5.1. Blood coagulation index assay

For blood clotting index (BCI) measuring, 15 mm by 15 mm gauzes were placed in a Petri dish and pre-warmed at 37 °C. Following the mixing of citrated blood and 0.2 M $CaCl_2$ in a 10:1 vol ratio to initiate the clotting after mixing the citrated blood with 0.2 M $CaCl_2$ at a volume ratio of 10:1 to initiate coagulation, 20 μL of recalcified blood was added and sandwiched between the gauzes. Blood was allowed to coagulate for 1, 3, and 5 min at 37 °C, blocking coagulation by the addition adding of 10 ml of distilled water without destroying the clot. Non-clotted erythrocytes would rupture hemolysis to release hemoglobin into the water. OD of the hemoglobin solution at different clotting time, OD (t) was determined by a spectrophotometer at 540 nm. The OD of 20 μL blood in 10 ml distilled water, OD (0) was used as reference. Blood coagulation index (BCI) was calculated as OD (t)/OD (0) [74].

For BCI measuring in harsh environments, the sample, consisted of a gauze layer, a PCM layer and an aerogel layer, was placed on a heating or cooling plate and recalcified blood was added to the gauze layer. Here, the AWNSA@G comprised a layer of 2 cm coated gauze and two layers of 10 cm coated gauze. Blood was allowed to coagulate between the gauze for 1, 3, and 5 min and then the gauze was gently transferred to a Petri dish and 10 ml of distilled water was added to terminate the coagulation. The remaining procedures were as described previously.

2.5.2. Plasma clotting assay

The procoagulant effect of gauze was also assessed by *in vitro* plasma clotting [65]. Firstly, plasma was collected from fresh rat blood by centrifugation at 2000 rpm for 20 min. Then, 1 ml plasma was transferred to a 2 ml centrifuge tube containing gauze (size: 15 mm by 15 mm) and 0.2 M $CaCl_2$ was added in a 10:1 vol ratio. The tube was subsequently shaken at 37 °C. We define plasma clotting time as the time required for plasma to transform from a liquid state to a fibrin clot.

2.5.3. Platelets on gauze

Platelets on gauze was analyzed by SEM and LDH assay [74]. Platelets-rich plasma (PRP) was derived from centrifuging the blood in sodium citrate tube at 200 g for 15 min, and then 20 μL of PRP was added to a 24-well plate that contains gauze with a size of 10 mm × 10 mm at 37 °C. After incubated for 30 min, the gauze was washed by PBS for five times, and 500 μL of 1% Triton-100 was used to lyse platelets for 1 h. Lastly, the adhesive efficiency was analyzed by an LDH kit according to the manufacturer's instructions. For SEM observing, the sample was fixed with 2.5% (v/v%) Glutaraldehyde/PBS solution for 4 h. Then, it was rinsed twice with PBS, and subsequently dehydrated in a series of 10, 20, 40, 60, 80 and 100% (v/v%) ethanol/PBS solutions. Afterwards, the gauze was dried at 37 °C and then sputtered with gold before testing by SEM.

2.5.4. Activity of coagulation factors was detected by ELISA kits

The activity of coagulation factors in plasma was detected by ELISA kits. The nano-silica aerogel was sprayed onto the bottom of the Petri dish and then plasma was contacted with it for 5 min, with unsprayed Petri dish as control. The concentration of activated coagulation factor XII (FXIIa) was later determined by FXIIa ELISA kit according to the manufacturer's instructions.

For the detection of prothrombin activity under extremely hot and cold environments, plasma was exposed to −20, 70 and 37 °C for 1, 3 and 5 min, respectively, after which prothrombin fragment 1 + 2 concentrations were determined with an ELISA kit.

2.5.5. Blood clot on gauze was observed by SEM

The microscopic structure of blood clot on gauze was observed by SEM. 2 cm coated gauze and 10 cm coated gauze were trimmed to a size of 15 mm by 15 mm. Then, 20 μL of recalcified blood was added and sandwiched between these two gauzes, with normal gauze as control. After 5 min, the gauze was washed with PBS and fixed with 2.5% (v/v%) Glutaraldehyde/PBS solution for 4 h. Afterwards, it was rinsed, dehydrated, and dried before SEM testing.

2.6. Hemostasis evaluation in vivo

All experiments performed in our research were complied with the rules for the use and care of laboratory animals in Jiangnan University. The study was granted approval by the Animal Ethics Committee of Jiangnan University (Protocol JN. No 20220615S0801025). The femoral artery injured model was prepared as following [75]. Rats were randomly grouped and anesthetized by intraperitoneal injection of sodium pentobarbital at 40mg/kg. The fur was then removed from the thigh of rat to allow exposure of the femoral artery. Pre-weighted gauze was laid under the thigh. The artery then was transected by a scalpel. After 3 s of bleeding, pre-weighted gauze was applied to the injury with the consistent compression for 60 s. Successful hemostasis was achieved when the area of blood-stained gauze didn't enlarge and no additional blood leaked out. To observe the microscopic morphology, the blood-stained gauze after hemostasis was washed with PBS and fixed with 2.5% (v/v%) Glutaraldehyde/PBS solution. Then, it was rinsed, dehydrated, and dried before SEM testing.

2.7. Measurement of peeling force

Rats were anesthetized by intraperitoneal injection of sodium pentobarbital at 40mg/kg. The hair on back was removed with an electrical razor and Veet® hair removal cream, then disinfected by 75% alcohol. A 1 cm incision was made on each side of the rat's dorsal midline with a scalpel, and the gauze with a size of 15 mm by 30 mm was applied to the wound. Here, the AWNSA@G was formed by a layer of 2 cm coated gauze and a layer of 10 cm coated gauze. The peak peeling force was recorded using a digital push & pull tester at 1 h after treatment.

2.8. Statistical analysis

The data are present as the mean ± standard deviation (SD) and analyzed by one-way analysis of variance (ANOVA) and student t-test. $P < 0.05$ means significant difference. $P < 0.05$: *, $P < 0.01$: **, and $P < 0.001$: ***.

3. Results and discussion

3.1. Fabrication and characterization of hydrophobic modified nano-silica aerogel

A wide variety of aerogels are available, among which inorganic silica aerogel is the most used in thermal management. Nevertheless, its application in hemostasis is rarely investigated. In our work, nano-silica aerogel was synthesized in a simple and economic approach only by two steps [32]. (1) By sol-gel method without ion-exchange, we prepared silica hydrogel with sodium silicate as precursors. As shown in Fig. 1a, the hydroxyl groups of the silica particles undergo a condensation reaction to form a silica hydrogel. (2) Nano-silica aerogel was attained by mixing silica hydrogel with superhydrophobic modification agents at elevated temperature. In second process, HMDS and HMDSO convert hydroxyl groups on the surface of silica hydrogel into methyl groups (Fig. 1b), which was beneficial to inhibit the absorption of water and prevent the collapse of pore structure. This hydrophobic improvement will also lead to the potential hemostasis [35,36]. Subsequent to that, the aqueous phase in the pores of the nano-silica aerogel was expelled with the dispersion of residual HMDSO or HMDSO produced by the oxidation of HMDS. Meanwhile, the previously generated sodium ions dissolved in water were separated from the HMDSO/HMDS phase, avoiding the extra step of sodium ion replacement. After completing the above process, nano-silica aerogel was floated on top of the reaction solution due to hydrophobic effect. We obtained hydrophobic nano-silica aerogel with a high specific surface area of 355.3 m^2/g, which was detected by energy dispersive X-ray spectroscopy (EDS) with a sodium ion removal rate of 98.8% (Fig. 1c). We confirmed by FT-IR that the Si–OH group on the surface of the nano-silica aerogel was partially replaced by the Si-$(CH_3)_3$ group (Fig. 1d). The peak at 2961 cm^{-1} matches the –CH_3 group stretching vibrations and that at 845 cm^{-1} is assigned to the Si–C bond, which proves the existence of the -Si$(CH_3)_3$ groups [32,37]. The surface properties of the nanoparticles can affect the agglomeration of the particles, and organosilanes modified silica is more prone to agglomeration [38]. In our research, particle size analysis showed that the prepared aerogel was homogeneous nanoparticles mainly due to ultrasonic dispersion (Fig. 1e). In contrast, SEM observed some aggregation of silica aerogel nanoparticles and thus the shape was not completely uniform (Fig. 1f and Fig. S1). Additionally, the pore structure of the silica aerogel could not be identified by SEM because of the physical weak phase interactions existing between secondary silica particles in porous silica prepared by sol-gel technology, which is easily disrupted by high voltage electron beams [39,40]. We also could not recognize significant pore structure of silica aerogel in the TEM images (Fig. 1g and Fig. S2), which has been indicated in other researches [41,42]. The nitrogen adsorption and desorption method was

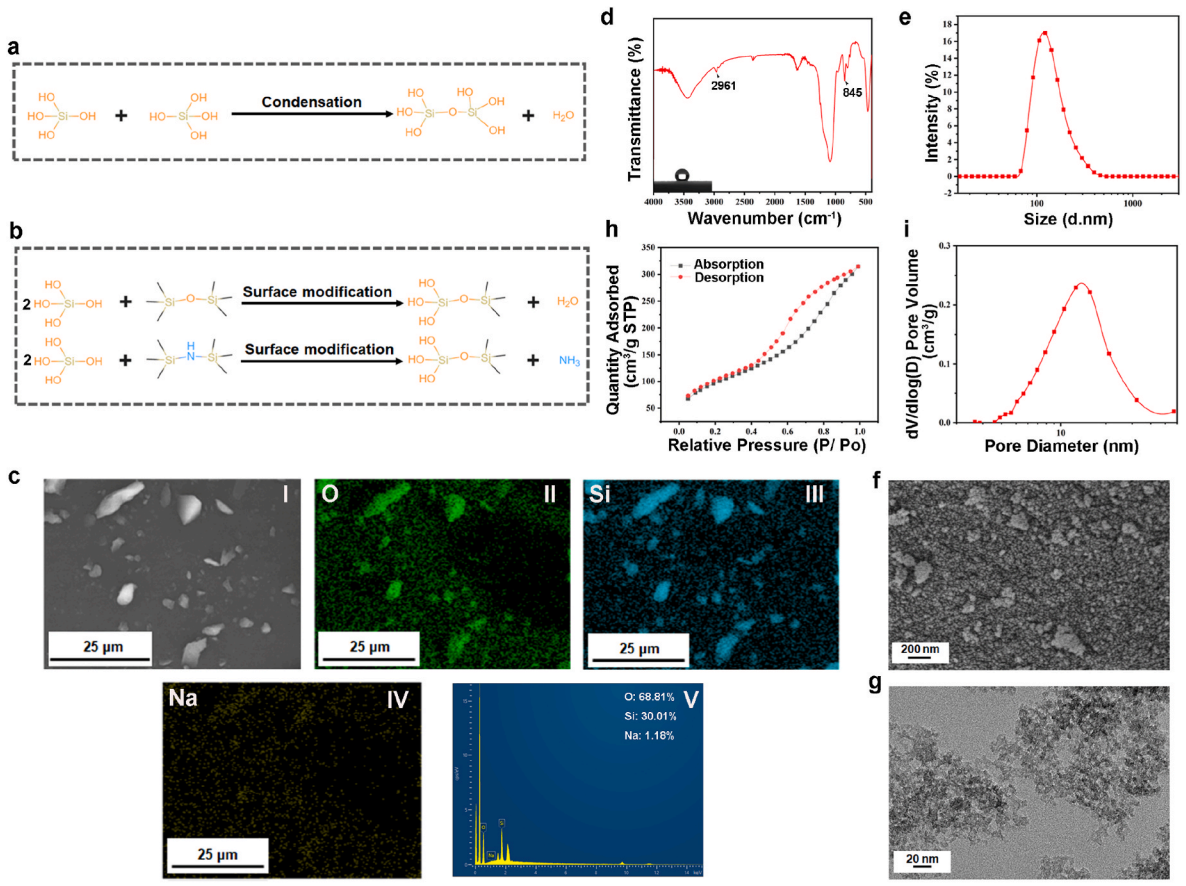

Fig. 1. (a) Condensation mechanism of silica particles; (b) surface modification reactions of silica particles; (c) EDS analysis (I was SEM image, II- IV were elemental maps, and V was spectrum) of nano-silica aerogel; (d) FT-IR spectrum and image of water contact angles test (inset) for nano-silica aerogel; (e) particle size analysis for the nano-silica aerogel; (f) SEM image of the nano-silica aerogel; (g) TEM image of the nano-silica aerogel; (h) nitrogen adsorption−desorption curve of the nano-silica aerogel; (i) pore size distribution (PSD) of the nano-silica aerogel.

further employed to characterize porous structure of nano-silica aerogel. Since the N_2 adsorption-dissociation curves of nano-silica aerogel was typical type IV curves according to IUPAC classification, suggesting that they had the characteristics of mesoporous materials (Fig. 1h). The thermal conductivity depends on the molecular vibrations in the air [43]. The pore size of nano-silica aerogel was only 2–50 nm (Fig. 1i), smaller than the mean free path of air (70 nm in the atmosphere) [32], suggesting its excellent thermal insulation properties.

3.2. Preparation and characterization of hydrophobic nano-silica aerogel-coated gauze

Inorganic materials and organic polymers are the two main categories of hemostatic materials commonly used today. Each of these materials has limitations when used alone, including unstable performance, poor environmental suitability, high cost, and potential safety risks. Some efforts have been made to optimize the efficiency of hemostasis, strengthening the advantages and minimizing the disadvantages by combining polymers and inorganic materials [34]. Based on the silica component, high surface area and porosity, and appropriate pore size, nano-silica aerogel is prospective for utilization in uncontrolled hemorrhage. Furthermore, the hydrophobic nature of aerogel can be beneficial in slowing down the bleeding rate by repelling blood. In our research, hydrophobic nano-silica aerogel was sprayed onto the surface of gauze at different distances to fabricate gauzes with variable wettability (Scheme b). The gauzes sprayed with aerogel at distances of 15, 10, 5 and 2 cm were assigned as 15 cm, 10 cm, 5 cm, and 2 cm.

3.2.1. Chemical composition and surface structure of hydrophobic nano-silica aerogel coated-gauze

The amount per unit area (APUA) of nano-silica aerogel on gauze (mg/cm^2) was examined, and the results demonstrated that the amount of nano-silica aerogel on the gauze increased significantly as the spray distance was reduced (Fig. 2a). We further determined the presence of nano-silica aerogel on gauze by FT-IR, SEM and EDS. As shown in Fig. 2b, with the decrease of spraying distance, the peak at 2961 cm^{-1} was gradually enhanced, indicating the increase of methyl groups from nano-silica aerogel. Meanwhile, the peak at 845 cm^{-1} also strengthened, indicating that the content of -Si $(CH_3)_3$ groups carried by nano-silica aerogel on the gauze was also increased. The SEM images showed obvious distinction between normal gauze and nano-silica aerogel-coated gauze, where nanoparticles were immobilized on the cotton fibers and could not fall from the fibers after repeated washing (Fig. 2c). In addition, more nanoparticles adhered to silica aerogel-coated gauze with a spray distance of 2 cm than 10 cm. We further analyzed the chemical compositions of nano-silica aerogel-coated gauze by EDS. It showed that silica was present on the surface of the coated gauze, while the normal gauze was not (Fig. 2d and e). Moreover, silica content on nano-silica aerogel-coated gauze with a 2 cm spraying distance was significantly higher than a 10 cm spraying distance.

3.2.2. Wettability, water vapor permeation and water uptake of gauze

The wettability of the gauze is essential for the absorption of blood and the adhesion of blood components. In this study, the wettability of the gauze was evaluated by adding 20 μL of SBF. As shown in Fig. 3a and Fig. S3, due to the siphoning effect of the gauze structure and the highly

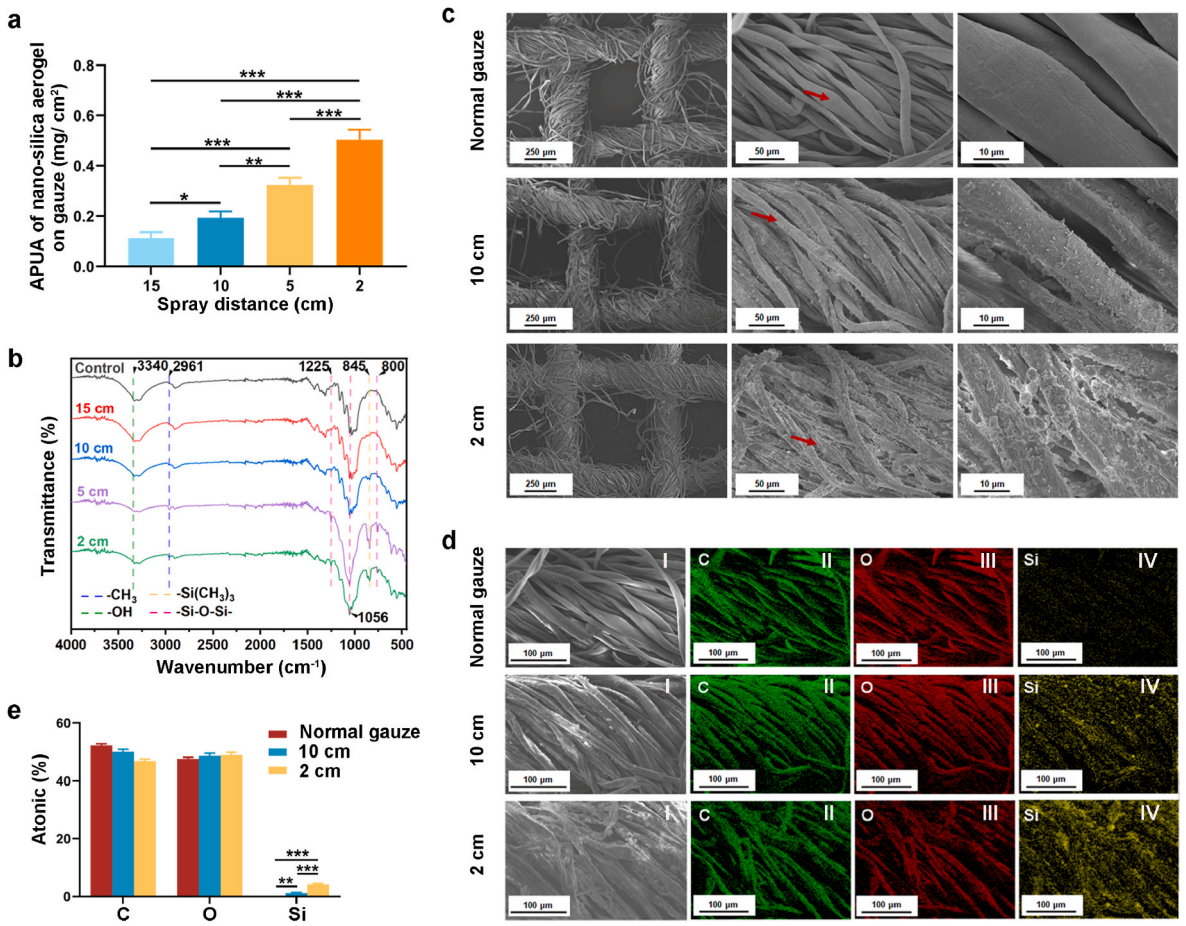

Fig. 2. (a) The amount per unit area (APUA) of nano-silica aerogel on gauze (n = 3); (b) FT-IR spectrums of hydrophobic nano-silica aerogel-coated gauzes with varied spray distance; (c) SEM image of hydrophobic nano-silica aerogel-coated-gauzes; (d) EDS analysis (I was SEM image, and II- IV were elemental maps) of hydrophobic nano-silica aerogel-coated gauze; (e) quantitative analysis on the elemental composition of aerogel coated-gauze (n = 3).

hydrophilic nature of the cotton fibers, water droplets that fell on the surface of normal gauze immediately diffused into the gauze. As the spraying distance decreased, the spread of the water droplets on the gauze gradually slowed down. At a spraying distance of 10 cm, it took 48 s for the droplets to spread into the gauze, and 76 s was required at 5 cm. However, when the spraying distance was 2 cm, the water droplets were difficult to diffuse into the gauze. Similarly, the coating of the nano-silica aerogel weakens the blood absorption efficiency of the gauze. We further added 200 μL of rat blood dropwise to the gauze to evaluate the effect of blood on the wettability of the gauze. In Fig. 3b, normal gauze obviously absorbed blood quickly. However, the blood spread slowly and was absorbed into the gauze fibers when it was dripped onto the silica aerogel-coated gauze at a spraying distance of 15 cm. A small volume of blood diffused into the nano-silica aerogel-coated gauze at a spraying distance of 10 cm. Furthermore, only a very minimal area of gauze was wetted with blood after 5 cm spraying, and the gauze couldn't be wetted after 2 cm spraying. SBF absorption experiments also showed that the water uptake of nano-silica aerogel-coated gauze decreased as the spray distance was reduced (Fig. 3c). Proper water vapor transmission is one of the important characteristics for wound dressings [44], we found that, the vapor transmission rate of the gauze was not influenced by the nano-silica aerogel coating (Fig. 3d). Together, these results suggested that the gauze modified with hydrophobic nano-silica aerogel was promising for improving the efficiency of hemostasis through controlling blood movement and reducing blood loss.

3.2.3. *Unidirectional fluid pumping effect of the hydrophobic-hydrophilic composite gauze*

Biofluid management around the wound is a pre-requisite for wound repair, including control of bleeding and removal of excess biofluids. Conventional dressings can absorb wound fluid, but they inevitably retain too much biofluid at the wound site owing to their inherent hydrophilicity [45]. The residual biofluid continues to hydrate the wound and impairs the healing process [46]. Recently, asymmetric wetting materials with varying wetting properties on different sides have shown efficient biofluid management capabilities, for example, a single-sided fluorinated cotton fabric membrane [47], polycaprolactone/quaternized chitosan/polyvinyl alcohol nanofibrous aerogel [37], and hydrophilic cotton microfibers deposited with a hydrophobic polyurethane nanofiber array [48]. Herein, we sprayed the hydrophobic nano-silica aerogel onto the top layer of the gauze, while the bottom layers remained hydrophilic, trying to construct an asymmetric wetting dressing. To demonstrate the unidirectional fluid transfer capacity of the modified gauze, a model with a continuous SBF (labelled by sodium fluorescein) dropping out from a syringe via a micro-syringe pump was established to simulate wound exudation. The transport process of green SBF onto gauze was monitored by a camera under UV light (λ = 254 nm). As shown in Fig. 4a and Movie S1, when the droplets fell onto the normal gauze, they spread rapidly and as the droplets continued to fall, the whole layers of gauze were wetted with green SBF. For the gauze with hydrophobic nano-silica aerogel spraying onto the top layer (gauze with hydrophobic top layer), due to the strong repulsion of nano-silica aerogel, SBF hardly contacted with hydrophilic cotton fibers and retained between the hydrophobic nano-silica

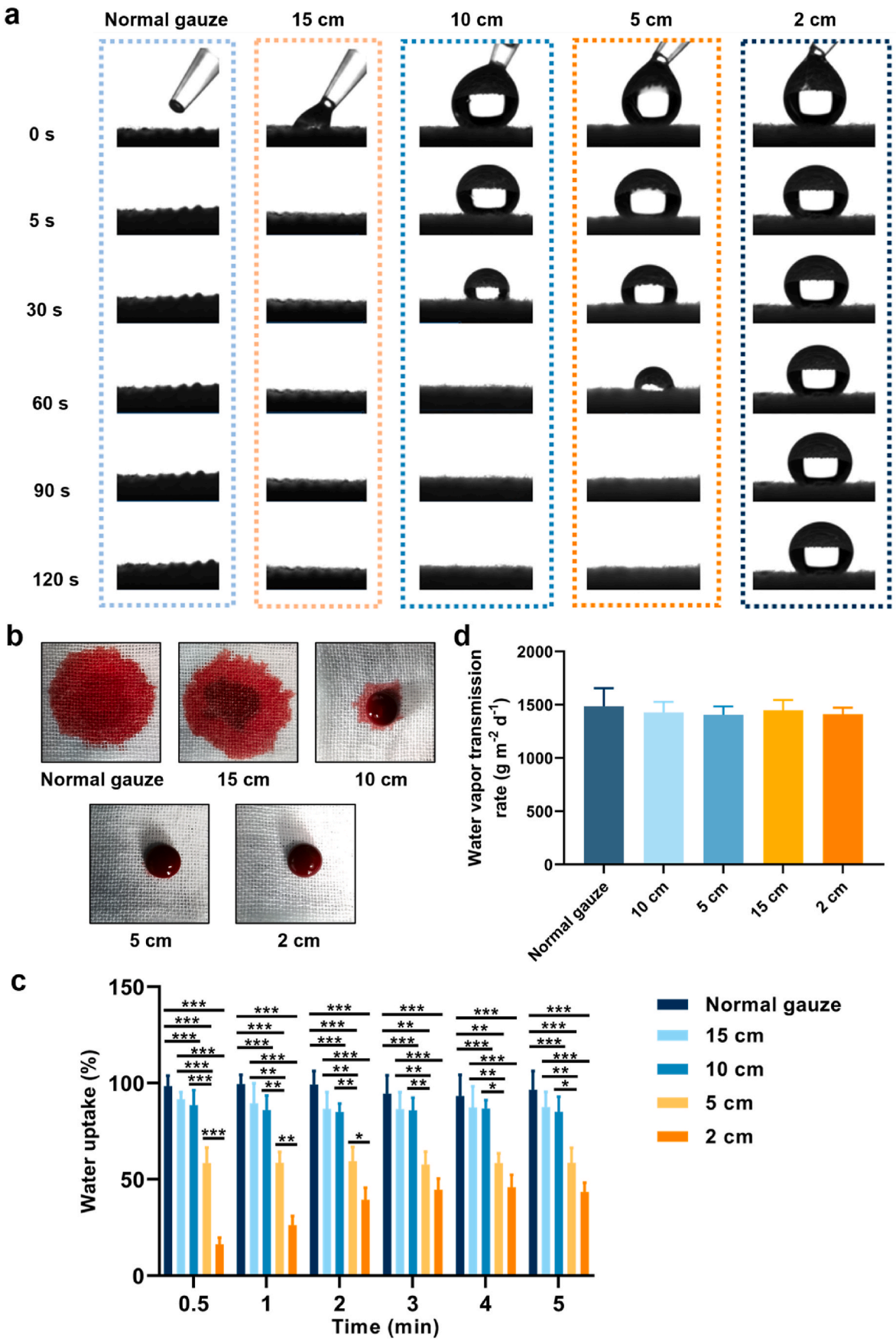

Fig. 3. (a) SBF wettability of gauzes; (b) blood wettability of gauzes; (c) water uptake of gauzes (n = 3); (d) water vapor permeation rate of gauzes (n = 3).

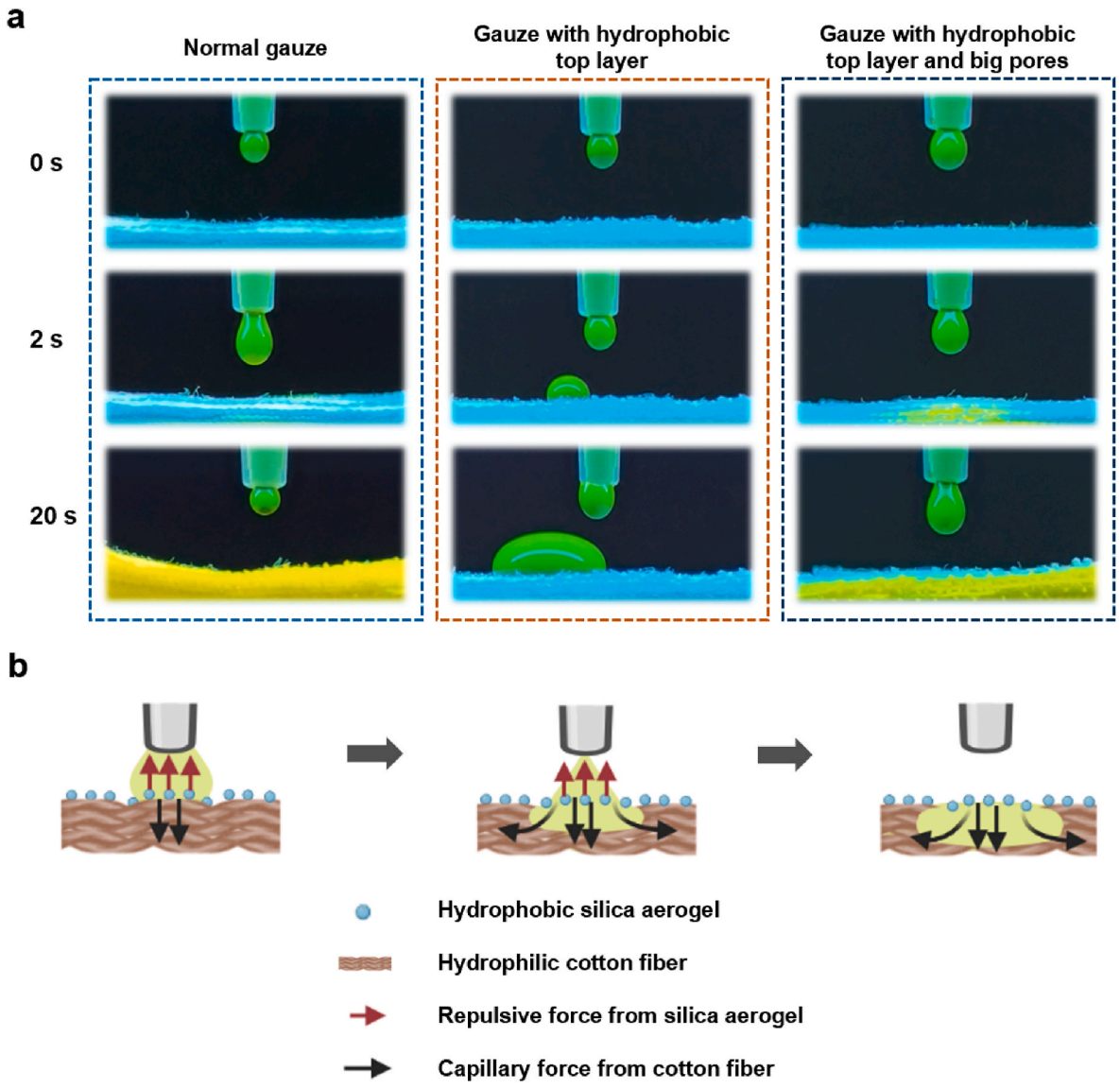

Fig. 4. (a) The transmission process of the SBF droplet (tagged with 1% sodium fluorescein) contacting with gauzes under UV light; (b) graphic illustration of the unidirectional liquid pumping mechanism.

aerogel-coated gauze and the syringe (Movie S2). Considering the capillary force of cotton fibers on fluid absorption, we increased its pore size by removing part of the filaments of the hydrophobic layer of gauze (gauze with hydrophobic top layer and big pores) (Fig. S4), so that the SBF was able to contact with the hydrophilic cotton fibers of the bottom layers, creating a hydrophobic-hydrophobic contact point. Droplet containing green SBF could quickly pass through the hydrophobic layer of the dressing and spread in the hydrophilic layer below (Movie S3). During this process, the hydrophilic layers of the asymmetric wetting material work as a pump [48], so it is called the self-pumping effect of the asymmetric wetting gauze. As the dropping SBF continued, the self-pumping process proceeded unidirectionally from hydrophobic to hydrophilic side. Hydrophobic top gauze layer was not wetted by green SBF, because of the repulsion by nano-silica aerogel and wicking by capillary action of hydrophilic cotton fibers (Fig. 4b). This phenomenon demonstrated the unique unidirectional fluid transport effect of asymmetric wetting gauze.

Supplementary data related to this article can be found at https://doi.org/10.1016/j.bioactmat.2023.02.017.

3.3. Biocompatibility of hydrophobic nano-silica aerogel-coated gauze

Good biocompatibility is a prerequisite for hemostatic applications of the materials. The hemolysis assay is well established method for assessing the hemocompatibility of biomaterials *in vitro* [49,50]. Diluted erythrocyte suspension was added to the centrifuge tubes, containing sprayed gauze at a distance of 2 cm for the experimental group or normal gauze for the control group, and dH_2O or PBS was added to the centrifuge tubes for the positive control and negative control, respectively. The macroscopical view of centrifugally obtained supernatants was presented in Fig. 5a. The nano-silica aerogel-coated gauze group with a spray distance of 2 cm showed pale yellow color similar to the normal gauze group and the negative control group, while the positive control group with the addition of dH_2O showed a bright red color due to hemolysis. As demonstrated in Fig. 5b, the quantitative analysis of the hemolysis rate showed that the hemolysis rate of nano-silica aerogel--coated gauze was comparable to normal gauze, only 0.7%, which was in compliance with confines of ASTMF756 (American Society for Testing and Materials).

Cytocompatibility is also an important indicator for the toxicity assessment of biomaterials *in vitro* [51,52]. In our research, extracts

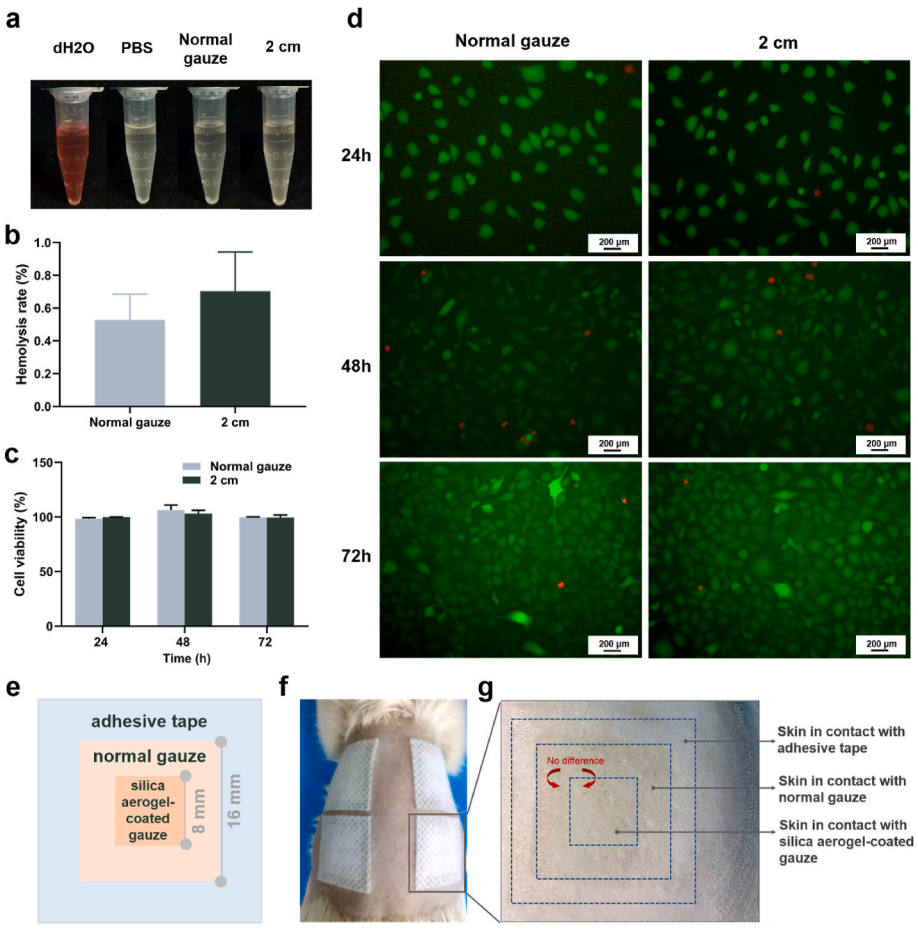

Fig. 5. (a) Macroscopical view of centrifugally obtained supernatants; (b) hemolysis rate of nano-silica aerogel-coated gauze (n = 3); (c) cell viability measured by CCK8 assay (n = 3); (d) images of live/dead cell staining; (e) illustration of the prepared sample for skin compatibility testing; (f) four samples were applied to the skin of the rat's back; (g) skin aera after 12 h of contact with the prepared sample.

incubation and direct contact testing were used to assess the cytocompatibility of gauzes. The results demonstrated that L929 cells maintained high cell viability after incubated with the extracts of nano-silica aerogel-coated gauze for 24, 48 and 72 h, comparable to the normal gauze (Fig. 5c). Cells in direct contact with the nano-silica aerogel-coated gauze also maintained the same good cell morphology and viability as the normal gauze (Fig. 5d and Fig. S5).

In addition, *in vivo* skin compatibility was assessed by applying the material onto the skin of rat's back with clinical adhesive tape for 12 h (Fig. 5e and f). Afterwards, the gauze was removed and the skin under the nano-silica aerogel coated-gauze was observed to be the same as that under the normal gauze, no swelling or erythema (Fig. 5g). These results suggest the excellent biocompatibility of silica aerogel-coated gauze as hemostatic agent.

3.4. Blood coagulation of gauze in vitro

BCI was used to determine the clotting ability of the gauze [26]. 20 μL of recalcified whole blood was applied between gauzes and allowed to clot over a period of time (Fig. 6a). Then, 10 ml of dH_2O was added to block the clotting. Erythrocytes not caught in the clot would release free hemoglobin into the water. Thus, a lower hemoglobin concentration means a smaller BCI value and a stronger clotting capacity. Compared with normal gauze, all nano-silica aerogel-coated gauzes showed lower BCI values. Among them, the nano-silica aerogel-coated gauze with a spray distance of 10 cm showed the lowest BCI value and therefore fastest coagulation, regardless of whether the gauze was in contact with recalcified blood for 1 min, 3 min or 5 min. For the nano-silica aerogel-coated gauze with a spray distance of 2 cm, its BCI value was not significantly lower than that of normal gauze at 1 min, but at 5 min, the BCI value was statistically smaller than normal gauze. It is possible that due to the strong hydrophobicity of the nano-silica aerogel-coated gauze with a 2 cm spraying distance, at 1 min the nano-silica aerogel and the gauze were in less contact with the blood, making it hard to perform its procoagulant effect. At 5 min, by contrast, the gauze was in sufficient blood exposure and therefore capable of enhancing clotting (Fig. 6b). In addition, we examined the effect of nano-silica aerogel-coated gauze on the clotting time of plasma *in vitro*. The plasma clotting time of nano-silica aerogel coated-gauzes with spray distance of 10 cm, 5 cm, and 2 cm, was significantly shorter than normal gauze (Fig. 6c–e). These results demonstrate the remarkable *in vitro* blood coagulation properties of nano-silica aerogel-coated gauze.

3.5. Hemostasis efficiency of gauze in vivo

3.5.1. Evaluation of hemostasis in injured femoral artery model

In trauma treatment, rapid control of bleeding in a very short period of time remains one of the most demanding requirements [53]. We found nano-silica aerogel-coated gauze with a spraying distance of 10 cm exhibited the best *in vitro* procoagulant effect, and gauze with a spraying distance of 2 cm was strongly repulsive to blood, which may facilitate *in vivo* hemostasis [36]. Then we evaluated their hemostasis efficiency in injured femoral artery model in rats (Fig. 7a). The hemostatic performance of different gauzes was quite variable (Fig. 7b–e, Movie S4-7). After the femoral artery was transected, constant manual pressure was applied on the wound with gauzes for approximately 60 s.

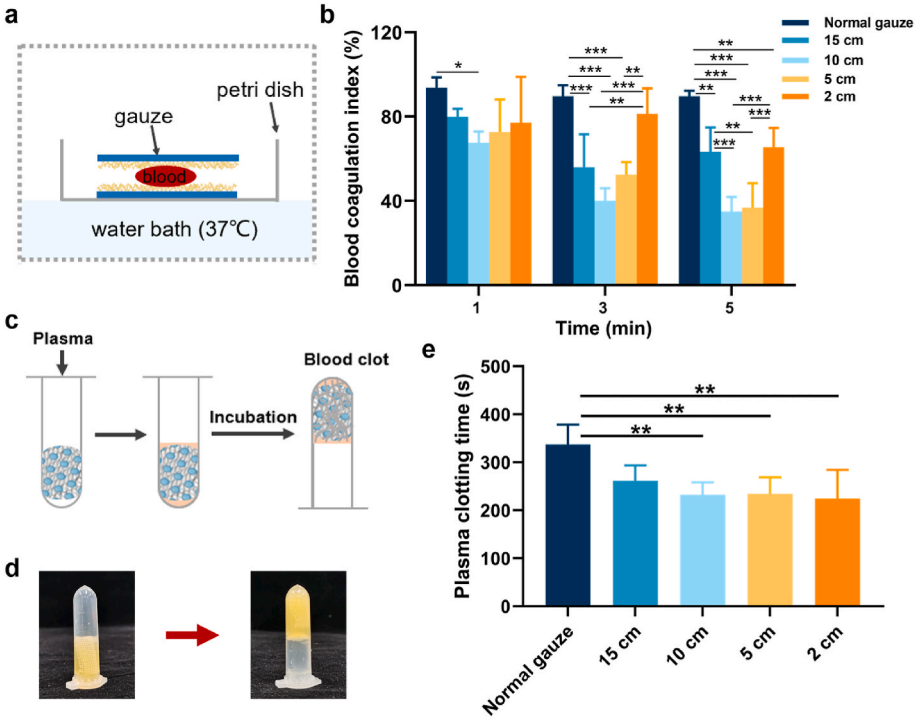

Fig. 6. (a) Schematic illustration of whole blood clotting test of gauzes; (b) blood coagulation index of gauzes (n = 5); (c) illustration of plasma clotting test; (d) image of liquid plasma transformed into coagulation formation; (e) the time of plasma clotting (n = 5).

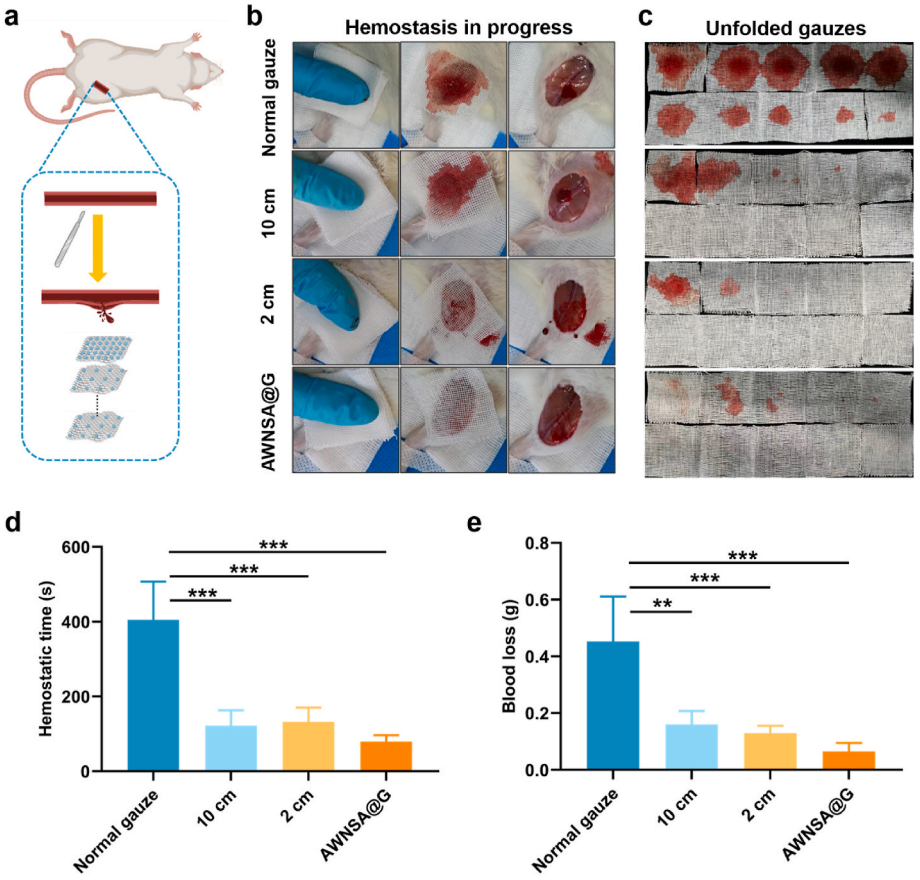

Fig. 7. (a) Schematic illustration of hemostasis process of nano-silica aerogel coated-gauze in rat femoral artery injury; (b) images of hemostasis in process; (c) laminated layers of gauze were unfolded; (d) statistical graph of hemostatic time in rats treated with normal gauze versus nano-silica aerogel coated-gauze (n = 4); (e) statistical graph of total blood loss in rats treated with normal gauze versus nano-silica aerogel coated-gauze (n = 4).

Then, the top layers of gauze were removed, leaving only the bottom layer attached to the wound, and the bleeding was observed. If the wound was still bleeding, continued constant compression with gauzes. At 10 min, removed all the gauze and observe whether it caused secondary bleeding. The hemostatic time of the nano-silica aerogel-coated gauze with 10 cm and 2 cm of spraying distance was 122 s and 132 s, respectively, significantly lower than the 405 s of the normal gauze in rat femoral artery injury model (Fig. 7d). Furthermore, as shown in Fig. 7e, the blood loss of coated gauze with 10 cm and 2 cm of spraying distance was about 0.1602 g and 0.1298 g respectively, both remarkably less than

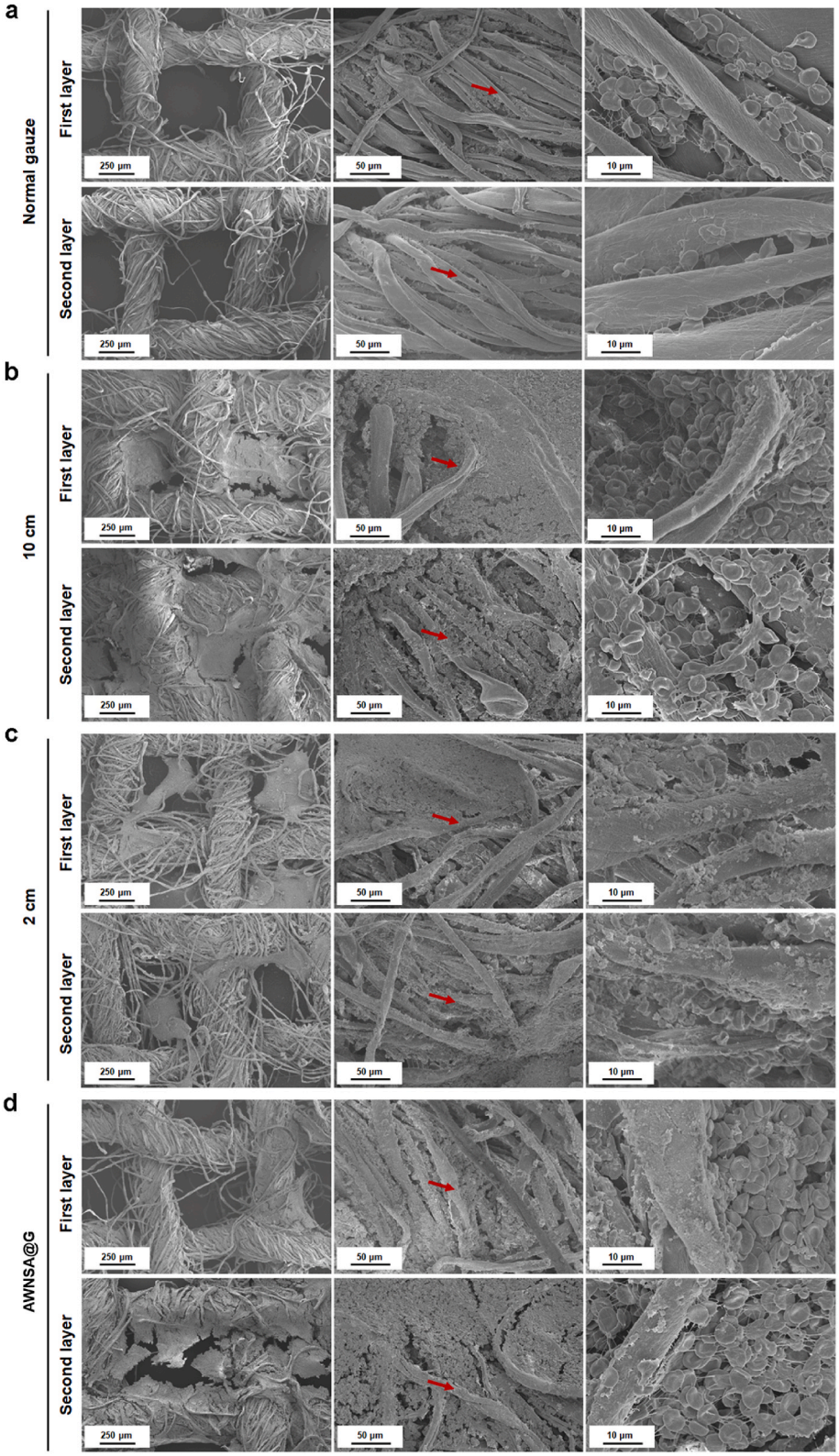

Fig. 8. Erythrocytes on: (a) normal gauze; (b) nano-silica aerogel-coated gauze with a spray distance of 10 cm; (c) nano-silica aerogel-coated gauze with a spray distance of 2 cm; (d) asymmetric wetting nano-silica aerogel-coated gauze (AWNSA@G).

the 0.4528 g of normal gauze. However, secondary bleeding was found after removal of the nano-silica aerogel-coated gauze at a spray distance of 10 cm, similar to normal gauze. Due to the strong hydrophobicity of the coated gauze with a 2 cm of spray distance, adhesions were prevented and its removal didn't cause rebleeding. But blood seeped out of the interface between gauze and tissue when the strongly hydrophobic gauze came into contact with the wound (Fig. 7b). In view of the effect of asymmetric wetting properties in unidirectional fluid pumping, a combination of 2 cm coated gauze and 10 cm coated gauze was considered to form an asymmetric wetting nano-silica aerogel-coated gauze (AWNSA@G) for hemostasis in rat femoral artery injury. A layer of 2 cm coated gauze was applied as an inner layer in direct touch with the wound to prevent adhesions and secondary bleeding, while nine layers of the 10 cm coated gauze were used as the upper layers to accelerate clotting. Surprisingly, the hemostasis time and blood loss of the AWNSA@G were 80 s and 0.0655 g, which were both less than the 2 cm and 10 cm coated gauze applied alone. In addition, no blood was observed to leak from the seam and secondary bleeding hardly happens when the gauze was removed at 10 min. Unlike *in vitro*, where extra pores in the strong hydrophobic layer are required to achieve the unidirectional fluid pumping effect of the asymmetric wetting gauze, blood can diffuse across the strong hydrophobic layer into the weak hydrophobic layers of the AWNSA@G without removing any filaments, mainly due to the effect of manual compression.

Supplementary video related to this article can be found at https://doi.org/10.1016/j.bioactmat.2023.02.017

3.5.2. *Microstructure of gauze after applying to a rat femoral artery injury*

Erythrocyte aggregates and fibrin networks are crucial components of the blood clot in controlling hemorrhage [54]. During the clot formation, fibrinogen is transformed into fibrin by thrombin. The fibrin monomers then interconnect and aggregate to form fibrin polymer network that entraps the erythrocytes and forms the clot [55]. To understand the interaction of erythrocyte, fibrin, blood clot and the silica aerogel-coated gauze, the blood-stained gauze was investigated after applying to a rat femoral artery injury model for 10 min. In Fig. 8a–d, compared with normal gauze, significant blood clots were observed in the cotton fibers or pores of the first and second layers of nano-silica aerogel-coated gauzes, which were sprayed at a distance of either 2 cm or 10 cm or a combination of both. In addition, erythrocytes

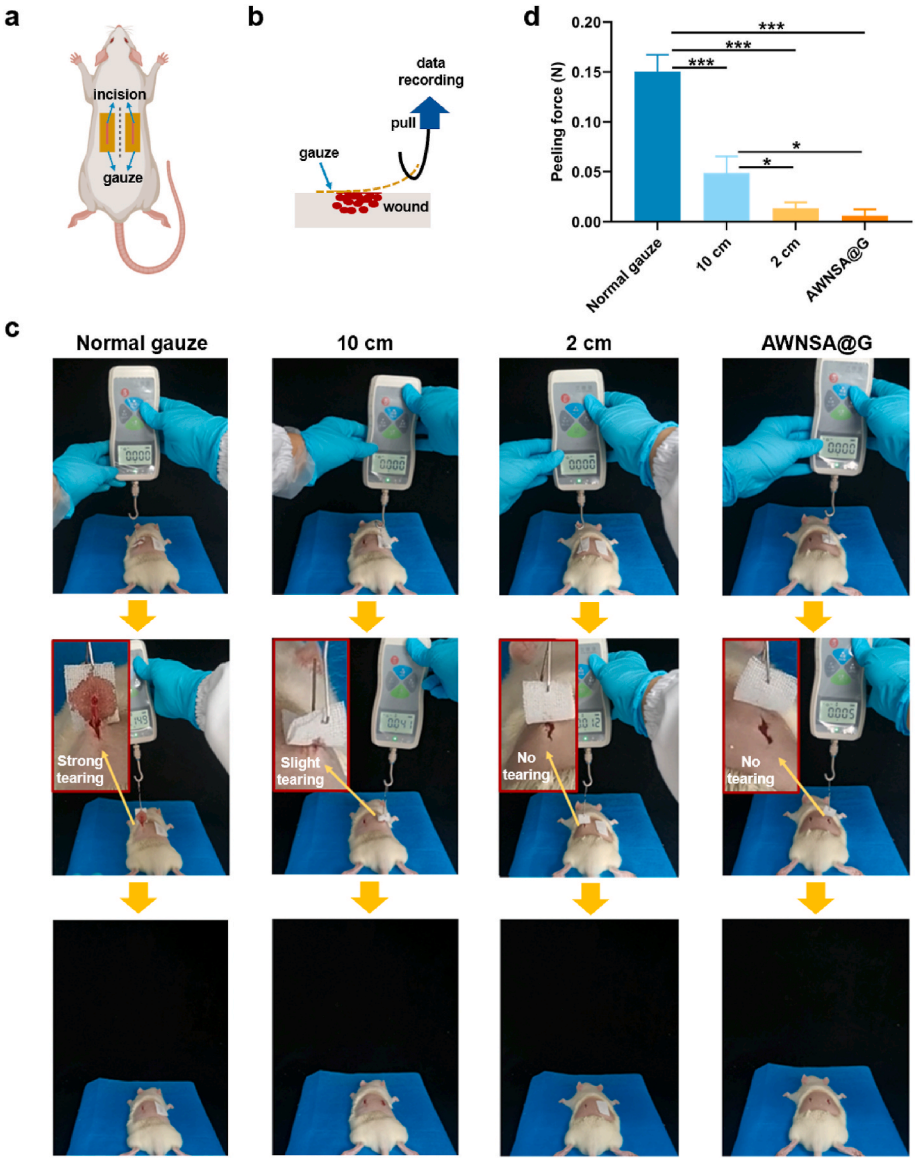

Fig. 9. (a) Illustration of the gauze applied onto the wound of the rat back; (b) schematic method for measuring peeling force; (c) the experimental procedure for peeling the gauze from the wound site, (d) the peak peeling force of different gauzes (n = 3).

entrapped by fibrin polymer network was adhered on fiber of silica aerogel-coated gauzes and maintained normal concave disk shape, suggesting that sprayed nano-silica aerogel does not affect the physiological state of erythrocytes. These phenomena demonstrate the potential pro-coagulant effect of nano-silica aerogel-coated gauze.

3.6. Peeling force of the gauze

The removal of dressings after hemostasis is also one of the current challenges for hemostatic materials [56]. When hydrophilic materials are applied, the blood clot after hemostasis is firmly adhered to the material and forced removal often tears the wound, causing pain and secondary bleeding [26]. To verify the easy peeling of our modified gauze, we created the back-bleeding model in rats. An incision was made on each side along the midline of the rat's back and gauze was attached to it (Fig. 9a). After 1 h, the gauze was removed from the wound and the maximum peeling force during this process was recorded (Fig. 9b). As demonstrated in Fig. 9c and d, the peeling force of the 2 cm-coated gauze and the AWNSA@G was approximately 11.3 and 23.8 times lower than that of the normal gauze, respectively, and their removal did not cause any tearing on the wound. Nevertheless, a slight stretching of the incision was observed with the removal of the 10 cm-coated gauze. In contrast, normal gauze caused stronger wound tearing during removal. Overall, our designed AWNSA@G was of easy peeling and minimized tearing of the wound, avoiding pain and rebleeding.

3.7. Thermal management of the LBL structure in harsh environment

Aerogels usually have exceptionally low thermal conductivity because of highly porous properties. They are passively insulated, and

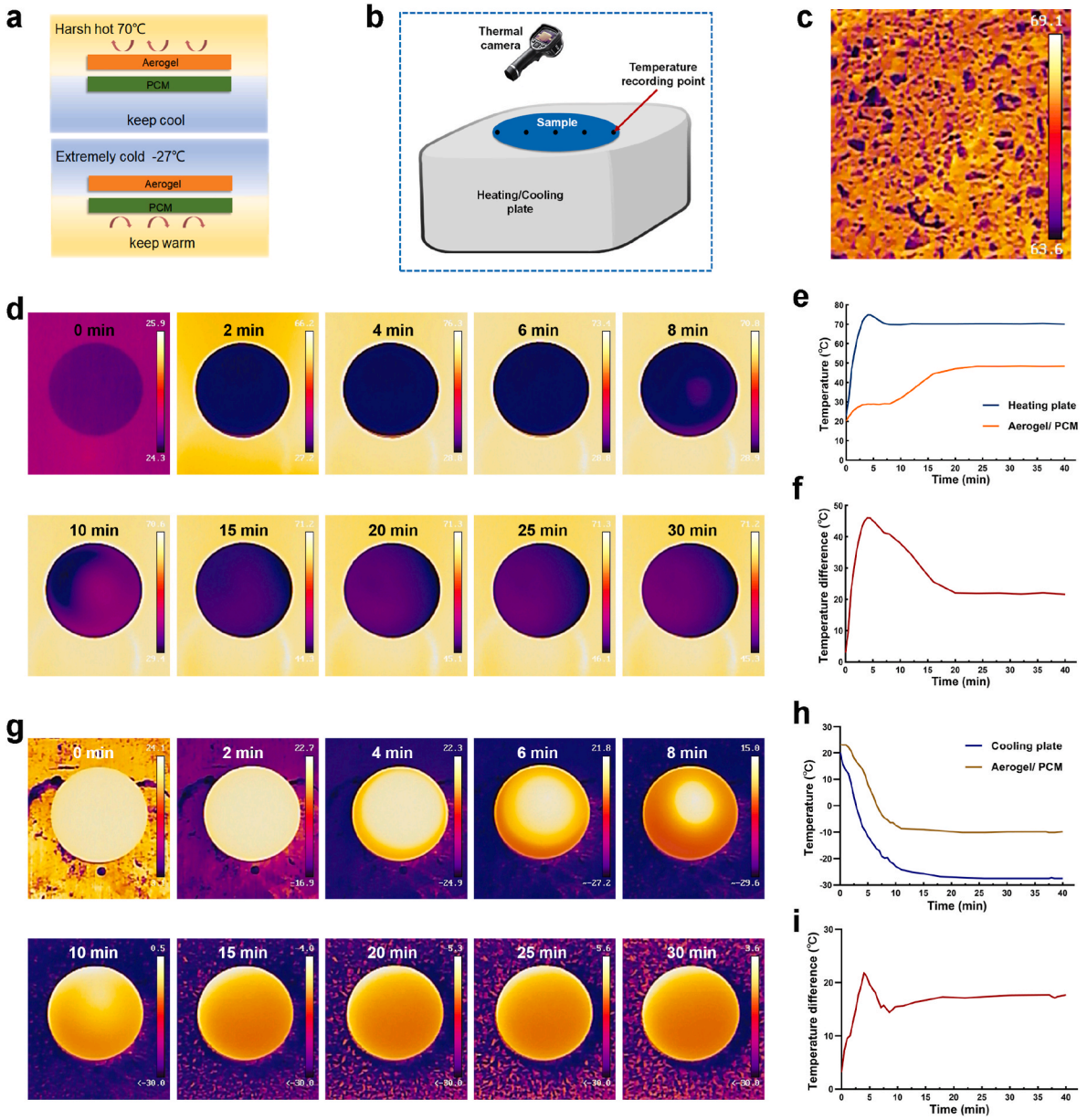

Fig. 10. (a) Schematic diagram of LBL structure assembling with nano-silica aerogel layer and PCM layer under extreme environments; (b) schematic illustration of the LBL structure tested on a heating/cooling plate; (c) infrared thermography image of summer ground surface; (d) infrared thermography image of the sample on a heating plate at indicated time points; (e) time-temperature curve of heating plate and LBL structure; (f) time-temperature difference curve of heating plate and LBL structure; (g) infrared thermography image of the sample on a cooling plate at indicated time points; (h) time-temperature curve of cooling plate and LBL structure; (i) time-temperature difference curve of cooling plate and LBL structure.

while combined with active temperature-regulating materials, they can have optimal temperature regulation [57,58]. PCMs are capable of absorbing or releasing latent energy from the substances over a limited temperature range [59]. However, the thermal insulation performance of PCMs relies on temperature and time, and they deliver minor and transient cooling/heating alleviation during temperature changes. While the composition of an aerogel layer with its low thermal conductivity and a high latent heat PCM layer can present excellent thermal insulation property with a prolonged working time. *N*-octadecane is a widely used PCM for its chemically inert, uncorrosive, readily available and free from unpleasant odors, with excellent thermal storage and release capabilities [60–62]. Thus, in our work, microencapsulated PCM of *n*-octadecane was applied to construct the inner layer of the LBL structure.

The performances of our thermal insulation structure in harsh conditions were examined (Fig. 10a and b). In extremely hot weather, 70 °C of the ground temperature can be easily achieved during the summer under constant sunlight radiation (Fig. 10c). Thus, to study the thermal insulation capacity of the samples, the LBL structure was placed on a heating plate heated to 70 °C and the temperature of the upper surface of the samples was monitored with a thermal infrared imager, and time-temperature curve was plotted. As shown in Fig. 10d–f, the temperature difference (ΔT) between the top surface of LBL structure and the heating plate could be up to 46 °C, indicating its excellent thermal insulation property. In addition, it took about 12.5 min for the upper surface temperature of the LBL structure to reach 37 °C, which is the optimal reaction temperature for a majority of enzymes [63]. Such a thermal conduction postponement is impressive as it completely meets the requirement of the "10 min gold" for rescue rule [64,65].

To determine the thermal management performance of the samples at extremely low temperature (−27 °C), the LBL structure were placed on a cooling plate cooled to −27 °C. As presented in Fig. 10g–i, the ΔT between the top surface of LBL structure and the cooling plate could reach up to 21.8 °C. Furthermore, the time to drop to 0 °C for the top surface temperature of the LBL structure was about 6.5 min. These results suggest that our design is highly effective for thermal management in both extremely hot and cold environments, thus available to maintain the relative stability of the wound microenvironment in harsh surroundings.

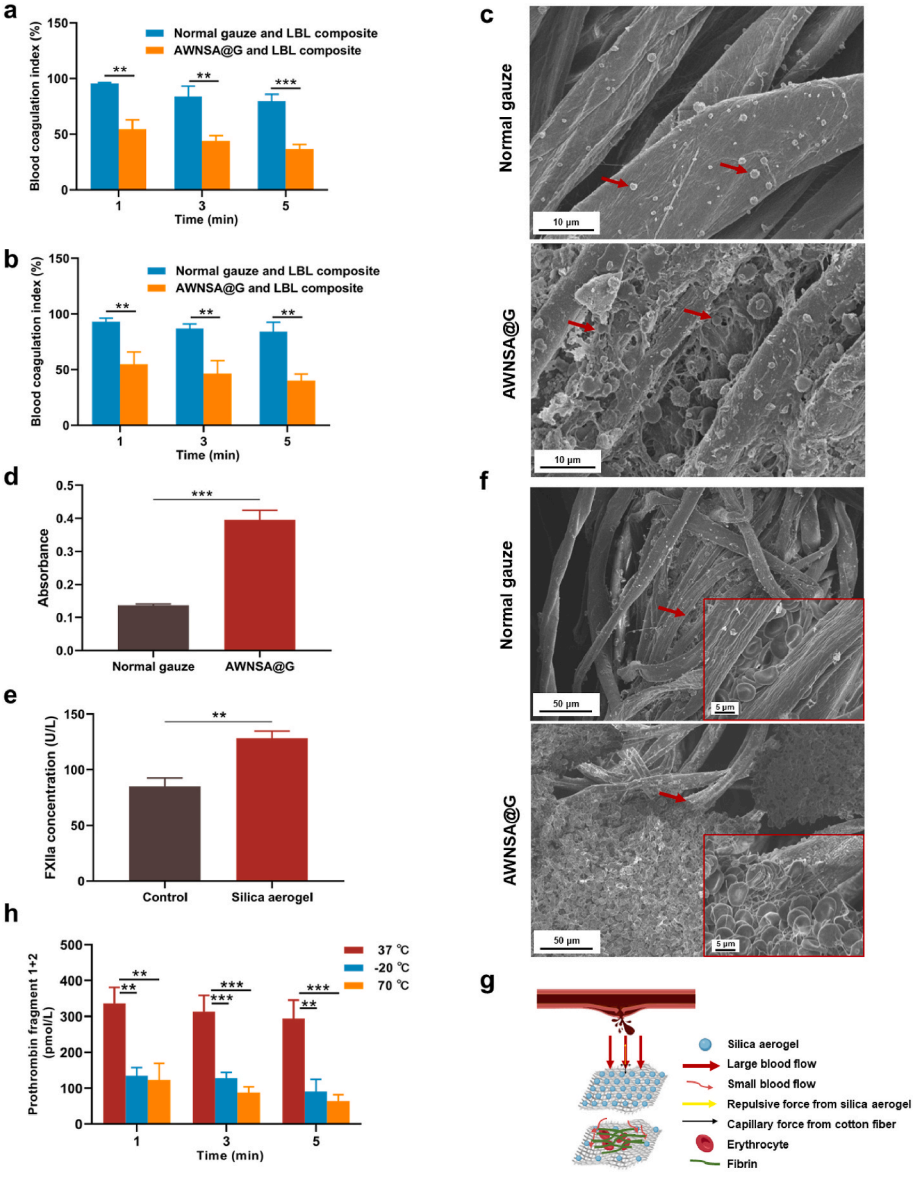

Fig. 11. (a) Blood coagulation of composites *in vitro* under harsh hot environment (70 °C) (n = 3); (b) blood coagulation of composites *in vitro* under harsh cold environment (−27 °C) (n = 3); (c) platelets (indicated by red arrows) on normal gauze and asymmetric wetting nano-silica aerogel-coated gauze (AWNSA@G) observed by SEM; (d) platelets adhesion determined by LDH assay (n = 3); (e) the effect of nano-silica aerogel on activation of coagulation factor XII (FXIIa) (n = 3); (f) *in vitro* coagulation of normal gauze and AWNSA@G observed by SEM; (g) schematic diagram of the hemostasis mechanism for AWNSA@G; (h) thrombin activity in extreme hot and cold environments (n = 3).

3.8. Hemostasis mechanism of AWNSA@G and LBL composite in extreme environments

We further validated the *in vitro* procoagulant effect of the AWNSA@G and LBL composite under extreme environments, with normal gauze and LBL composite as a comparison. The composites were placed on a heating or cooling plate and recalcified blood was then added to the gauzes of the composites. Coagulation was terminated at 1, 3, and 5 min respectively and the BCI was measured. As shown in Fig. 11a and b, the BCI of AWNSA@G and LBL composite was lower than that of the normal gauze and LBL composite in both harsh hot and cold conditions, indicating the excellent hemostasis performance of our composite even in extreme environments. Considering the physical effects of evaporation and freezing of water in the blood, we did not use single AWNSA@G or normal gauze as controls for the hemostasis test under harsh hot or cold conditions.

It is well established that adherence and aggregation of platelets at the injury site is a prerequisite for hemostasis [66,67]. Here, we examined the platelets on gauze by SEM and LDH assay. As shown in Fig. 11c, platelets with pseudopods and greater platelet aggregations were observed on AWNSA@G than on normal gauze. In addition, more LDH releasing was detected in the nano-silica aerogel-coated gauze (Fig. 11d), indicating that the AWNSA@G promoted platelets activation and adhesion over normal gauze. Initiation of the coagulation pathway is the final phase of hemostasis [68]. In this process, coagulation factors response in a complicated reaction cascade to form fibrin clot and prevent critical blood loss from the wound. Activation of coagulation factor XII (FXIIa) is an important cause of the endogenous coagulation cascade [69]. The outstanding hemostatic effects of silica-based materials, including the minerals zeolite and kaolin, have been attributed to the elevated concentration of FXIIa [70], and our nano-silica aerogel also increased the level of FXIIa (Fig. 11e). We further investigated the *in vitro* coagulation of AWNSA@G with SEM, and found that erythrocytes were entrapped in a fibrin network and a blood clot was formed in AWNSA@G (Fig. 11f). Therefore, the hemostatic mechanism of our AWNSA@G was illustrated in Fig. 11 g. When applying the gauze to a bleeding wound, the strong hydrophobicity of the first layer of nano-silica aerogel-coated gauze slowed down blood movement and promoted platelets activation and adhesion, while the nano-silica aerogel activated FXII, triggering the endogenous coagulation cascade. Simultaneously, a short period of manual compression drained the slowing blood flow to the weakly hydrophobic layer, allowing blood to wet, absorb, wick, and diffuse into the gauze, facilitating fast hemostasis.

In extreme environments, the protein components of coagulation factors in plasma can be impaired by cold or thermal stimuli, causing a reduction in the activity of coagulation factors and making hemostasis particularly challenging [20]. Prothrombin (coagulation factor II), a crucial factor for hemostasis, can be activated to create thrombin by the intrinsic or extrinsic coagulation cascade reaction, and subsequently transforming fibrinogen into fibrin monomer. When thrombin is generated, prothrombin fragment 1 + 2 is also produced as a by-product [71]. To clarify the effect of temperature on thrombin activity, plasma was exposed to 37 °C, −20 °C, and 70 °C for 1 min, 3 min, and 5 min respectively, and then the concentration of prothrombin fragment 1 + 2 was measured. We found that the concentrations of prothrombin fragment 1 + 2 in plasma incubated at −20 °C and 70 °C were significantly lower than that incubated at 37 °C (Fig. 11h), suggesting that thrombin activity was dramatically reduced in extreme environments. While our LBL structure, comprising a nano-silica aerogel layer and a PCM layer, exhibited efficient thermal management by remarkably delaying heat transfer. As a result, the LBL structure maintained the wound microenvironment at a relatively suitable temperature, protecting thrombin from hot and cold stimuli and thus assisting the AWNSA@G to achieve highly effective hemostasis in harsh conditions.

4. Conclusion

To conclude, we have constructed a composite wound dressing with thermal management performance for preventing bleeding wounds from hot or cold stimuli and achieving efficient hemostasis. The composite was a combination of AWNSA@G and a LBL structure, where the asymmetric wetting gauze includes a strong hydrophobic layer close to the wound and other weak hydrophobic layers, while the LBL structure consists of a PCM layer and a nano-silica aerogel layer. Our *in vivo* and *in vitro* results indicated that the composite wound dressing was ideal for hemostasis in harsh environments because of its temperature management property, less blood loss, shorter coagulation time and easy stripping. This research expands the applications of nano-silica aerogel in wound dressing design and has extensive implications for controlling massive bleeding in extremely hot/cold conditions.

Author credit statement

GL and MX designed the research concept and supervised the program. XJ and CH prepared and characterized the materials, XJ and FY conducted the animal experiments with the help of XL. PZ performed the thermal insulation study. FZ completed *in vitro* coagulation experiments. YL analyzed the data, and HL contributed to the mapping of the images. All authors wrote, reviewed and commented on the manuscript.

Ethical

All animal experiments performed in our research were complied with the rules for the use and care of laboratory animals in Jiangnan University. The study was granted approval by the Animal Ethics Committee of Jiangnan University (Protocol JN. No 20220615S0801025).

Declaration of competing interest

The authors declare that they have no known competing financial interests or personal relationships that could have appeared to influence the work reported in this paper.

Appendix A. Supplementary data

Supplementary data related to this article can be found at https://doi.org/10.1016/j.bioactmat.2023.02.017.

References

[1] B. Wallner, B. Schenk, P. Paal, M. Falk, G. Strapazzon, W.Z. Martini, et al., Hypothermia induced impairment of platelets: assessment with multiplate vs. ROTEM-an in vitro study, Front. Physiol. 13 (2022), 852182, https://doi.org/10.3389/fphys.2022.852182.

[2] M.-M. Yang, L. Wang, Y. Zhang, R. Yuan, Y. Zhao, J. Hu, et al., Establishment and effectiveness evaluation of a scoring system for exertional heat stroke by retrospective analysis, Mil Med Res 7 (2020) 40, https://doi.org/10.1186/s40779-020-00269-1.

[3] B.R. Kupchak, J.B. Kazman, J.L. Vingren, D.E. Levitt, E.C. Lee, K.H. Williamson, et al., Blood hemostatic changes during an ultraendurance road cycling event in a hot environment, Wilderness Environ. Med. 28 (2017) 197–206, https://doi.org/10.1016/j.wem.2017.05.002.

[4] M. Gaudard, E. Boissier, L. Talon, J. Douxfils, A.-F. Sapin, T. Sinegre, et al., Stability of coagulation parameters in plasma samples at room temperature after one freeze/thaw cycle, Int J Lab Hematol 44 (2022) 610–618, https://doi.org/10.1111/ijlh.13794.

[5] S. Zhu, S. Bennett, V. Kuek, C. Xiang, H. Xu, V. Rosen, et al., Endothelial cells produce angiocrine factors to regulate bone and cartilage via versatile mechanisms, Theranostics 10 (2020) 5957–5965, https://doi.org/10.7150/thno.45422.

[6] M.N. Sawka, E.F. Coyle, Influence of body water and blood volume on thermoregulation and exercise performance in the heat, Exerc. Sport Sci. Rev. 27 (1999) 167–218, https://doi.org/10.1249/00003677-199900270-00008.

[7] S. Hof, R. Truse, L. Weber, A. Herminghaus, J. Schulz, A.P.M. Weber, et al., Local mucosal CO(2) but not O(2) insufflation improves gastric and oral microcirculatory oxygenation in a canine model of mild hemorrhagic shock, Front. Med. 9 (2022), 867298, https://doi.org/10.3389/fmed.2022.867298.

[8] M. Caspers, N. Schäfer, B. Bouillon, V. Schaeben, M.C. Ciorba, M. Maegele, et al., Plasmatic coagulation profile after major traumatic injury: a prospective observational study, Eur J Trauma Emerg Surg Off Publ Eur Trauma Soc (2022), https://doi.org/10.1007/s00068-022-01971-6.

[9] J.B. Holcomb, N.R. McMullin, L. Pearse, J. Caruso, C.E. Wade, L. Oetjen-Gerdes, et al., Causes of death in U.S. Special Operations Forces in the global war on terrorism: 2001-2004, Ann. Surg. 245 (2007) 986–991, https://doi.org/10.1097/01.sla.0000259433.03754.98.

[10] H.R. Champion, R.F. Bellamy, C.P. Roberts, A. Leppaniemi, A profile of combat injury, J. Trauma 54 (2003) S13–S19, https://doi.org/10.1097/01.TA.0000057151.02906.27.

[11] L. Yu, X. Shang, H. Chen, L. Xiao, Y. Zhu, J. Fan, A tightly-bonded and flexible mesoporous zeolite-cotton hybrid hemostat, Nat. Commun. 10 (2019) 1932, https://doi.org/10.1038/s41467-019-09849-9.

[12] A.K. Lorentzen, C. Davis, L. Penninga, Interventions for frostbite injuries, Cochrane Database Syst. Rev. 12 (2020), https://doi.org/10.1002/14651858.CD012980.pub2. CD012980.

[13] M.J. Powell-Palm, J. Aruda, B. Rubinsky, Thermodynamic theory and experimental validation of a multiphase isochoric freezing process, J. Biomech. Eng. (2019), https://doi.org/10.1115/1.4043521.

[14] C.-Y. Zou, X.-X. Lei, J.-J. Hu, Y.-L. Jiang, Q.-J. Li, Y.-T. Song, et al., Multi-crosslinking hydrogels with robust bio-adhesion and pro-coagulant activity for first-aid hemostasis and infected wound healing, Bioact. Mater. 16 (2022) 388–402, https://doi.org/10.1016/j.bioactmat.2022.02.034.

[15] B. Orlandini, T. Schepis, A. Tringali, P. Familiari, I. Boškoski, F. Borrelli de Andreis, et al., Fibrin glue injection: rescue treatment for refractory post-sphincterotomy and post-papillectomy bleedings, Dig Endosc Off J Japan Gastroenterol Endosc Soc 33 (2021) 815–821, https://doi.org/10.1111/den.13857.

[16] H.Y. Jung, P. Le Thi, K.-H. HwangBo, J.W. Bae, K.D. Park, Tunable and high tissue adhesive properties of injectable chitosan based hydrogels through polymer architecture modulation, Carbohydr. Polym. 261 (2021), 117810, https://doi.org/10.1016/j.carbpol.2021.117810.

[17] J. Yu, Y. Feng, D. Sun, W. Ren, C. Shao, R. Sun, Highly conductive and mechanically robust cellulose nanocomposite hydrogels with antifreezing and antidehydration performances for flexible humidity sensors, ACS Appl. Mater. Interfaces 14 (2022) 10886–10897, https://doi.org/10.1021/acsami.2c00513.

[18] A. Surowiecka, J. Strużyna, A. Winiarska, T. Korzeniowski, Hydrogels in burn wound management-A review, Gels (Basel, Switzerland) 8 (2022), https://doi.org/10.3390/gels8020122.

[19] P. Song, H. Qin, H.-L. Gao, H.-P. Cong, S.-H. Yu, Self-healing and superstretchable conductors from hierarchical nanowire assemblies, Nat. Commun. 9 (2018) 2786, https://doi.org/10.1038/s41467-018-05238-w.

[20] A. Simpson, A. Shukla, A.C. Brown, Biomaterials for hemostasis, Annu. Rev. Biomed. Eng. 24 (2022) 111–135, https://doi.org/10.1146/annurev-bioeng-012521-101942.

[21] R.I. Litvinov, R.M. Nabiullina, L.D. Zubairova, M.A. Shakurova, I.A. Andrianova, J. W. Weisel, Lytic susceptibility, structure, and mechanical properties of fibrin in systemic lupus erythematosus, Front. Immunol. 10 (2019) 1626, https://doi.org/10.3389/fimmu.2019.01626.

[22] S.E. Stabenfeldt, M. Gourley, L. Krishnan, J.B. Hoying, T.H. Barker, Engineering fibrin polymers through engagement of alternative polymerization mechanisms, Biomaterials 33 (2012) 535–544, https://doi.org/10.1016/j.biomaterials.2011.09.079.

[23] W. Tian, H. Sun, Y. Zhang, J. Xu, J. Yao, J. Li, et al., Thermal adaptation occurs in the respiration and growth of widely distributed bacteria, Global Change Biol. 28 (2022) 2820–2829, https://doi.org/10.1111/gcb.16102.

[24] A. Verma, H. Singh, M.S. Anwar, S. Kumar, M.W. Ansari, S. Agrawal, Production of thermostable organic solvent tolerant keratinolytic protease from thermoactinomyces sp. RM4: IAA production and plant growth promotion, Front. Microbiol. 7 (2016) 1189, https://doi.org/10.3389/fmicb.2016.01189.

[25] Y. Shi, X. Ding, Y. Cao, H. Zhou, W. Yu, M. Liu, et al., Preparation and application of quick hemostatic gauze based on biomimetic mineralized thrombin, Biomater. Sci. 9 (2021) 6098–6107, https://doi.org/10.1039/d1bm00917f.

[26] Z. Li, A. Milionis, Y. Zheng, M. Yee, L. Codispoti, F. Tan, et al., Superhydrophobic hemostatic nanofiber composites for fast clotting and minimal adhesion, Nat. Commun. 10 (2019) 5562, https://doi.org/10.1038/s41467-019-13512-8.

[27] Z. Zhao, Y. Cui, Y. Kong, J. Ren, X. Jiang, W. Yan, et al., Thermal and mechanical performances of the superflexible, hydrophobic, silica-based aerogel for thermal insulation at ultralow temperature, ACS Appl. Mater. Interfaces 13 (2021) 21286–21298, https://doi.org/10.1021/acsami.1c02910.

[28] L. Wang, J. Feng, Y. Luo, Y. Jiang, G. Zhang, J. Feng, Versatile thermal-solidifying direct-write assembly towards heat-resistant 3D-printed ceramic aerogels for thermal insulation, Small Methods 6 (2022), e2200045, https://doi.org/10.1002/smtd.202200045.

[29] Y. Du, X. Zhang, J. Wang, Z. Liu, K. Zhang, X. Ji, et al., Reaction-spun transparent silica aerogel fibers, ACS Nano 14 (2020) 11919–11928, https://doi.org/10.1021/acsnano.0c05016.

[30] R. Wu, W. Mei, Y. Zhou, T. Bi, Q. Lin, Continuous dual-scale interpenetrating network carbon foam-stearic acid composite as a shape-stabilized phase change material with a desirable synergistic effect, ACS Appl. Mater. Interfaces (2022), https://doi.org/10.1021/acsami.2c08564.

[31] S. Becherini, M. Mitmoen, C.D. Tran, Natural sporopollenin microcapsules facilitated encapsulation of phase change material into cellulose composites for smart and biocompatible materials, ACS Appl. Mater. Interfaces 11 (2019) 44708–44721, https://doi.org/10.1021/acsami.9b15530.

[32] L. Liu, X. Shan, X. Hu, W. Lv, J. Wang, Superhydrophobic silica aerogels and their layer-by-layer structure for thermal management in harsh cold and hot environments, ACS Nano 15 (2021) 19771–19782, https://doi.org/10.1021/acsnano.1c07184.

[33] D. Li, J. Chen, X. Wang, M. Zhang, C. Li, J. Zhou, Recent advances on synthetic and polysaccharide adhesives for biological hemostatic applications, Front. Bioeng. Biotechnol. 8 (2020) 1–16, https://doi.org/10.3389/fbioe.2020.00926.

[34] Z. Chen, L. Han, C. Liu, Y. Du, X. Hu, G. Du, et al., A rapid hemostatic sponge based on large, mesoporous silica nanoparticles and: N -alkylated chitosan, Nanoscale 10 (2018) 20234–20245, https://doi.org/10.1039/c8nr07865c.

[35] Y. Liu, H. Niu, C. Wang, X. Yang, W. Li, Y. Zhang, et al., Bio-inspired, bio-degradable adenosine 5'-diphosphate-modified hyaluronic acid coordinated hydrophobic undecanal-modified chitosan for hemostasis and wound healing, Bioact. Mater. 17 (2022) 162–177, https://doi.org/10.1016/j.bioactmat.2022.01.025.

[36] H. He, C. Sun, Y. Weng, H. Huang, P. Ni, Y. Fang, et al., Catechol modification of non-woven chitosan gauze for enhanced hemostatic efficacy, Carbohydr. Polym. 286 (2022), 119319, https://doi.org/10.1016/j.carbpol.2022.119319.

[37] K. Zhang, X. Jiao, L. Zhou, J. Wang, C. Wang, Y. Qin, et al., Nanofibrous composite aerogel with multi-bioactive and fluid gating characteristics for promoting diabetic wound healing, Biomaterials 276 (2021), 121040, https://doi.org/10.1016/j.biomaterials.2021.121040.

[38] C. Bantz, O. Koshkina, T. Lang, H.-J. Galla, C.J. Kirkpatrick, R.H. Stauber, et al., The surface properties of nanoparticles determine the agglomeration state and the size of the particles under physiological conditions, Beilstein J. Nanotechnol. 5 (2014) 1774–1786, https://doi.org/10.3762/bjnano.5.188.

[39] J. Lin, G. Li, W. Liu, R. Qiu, H. Wei, K. Zong, et al., A review of recent progress on the silica aerogel monoliths: synthesis, reinforcement, and applications, J. Mater. Sci. 56 (2021) 10812–10833, https://doi.org/10.1007/s10853-021-05997-w.

[40] H. Zou, S. Wu, J. Shen, Polymer/silica nanocomposites: preparation, characterization, properties, and applications, Chem. Rev. 108 (2008) 3893–3957, https://doi.org/10.1021/cr068035q.

[41] X. Chen, B. Put, A. Sagara, K. Gandrud, M. Murata, J.A. Steele, et al., Silica gel solid nanocomposite electrolytes with interfacial conductivity promotion exceeding the bulk Li-ion conductivity of the ionic liquid electrolyte filler, Sci. Adv. 6 (2020), https://doi.org/10.1126/sciadv.aav3400 eaav3400.

[42] S. Wu, Z. Shan, L. Xie, M. Su, P. Zeng, P. Huang, et al., Mesopore controls the responses of blood clot-immune complex via modulating fibrin network, Adv. Sci. 9 (2022) 1–16, https://doi.org/10.1002/advs.202103608.

[43] T. Li, J. Song, X. Zhao, Z. Yang, G. Pastel, S. Xu, et al., Anisotropic, lightweight, strong, and super thermally insulating nanowood with naturally aligned nanocellulose, Sci. Adv. 4 (2018) eaar3724, https://doi.org/10.1126/sciadv.aar3724.

[44] T. Khaliq, M. Sohail, S.A. Shah, A. Mahmood, M. Kousar, N. Jabeen, Bioactive and multifunctional keratin-pullulan based hydrogel membranes facilitate re-epithelization in diabetic model, Int. J. Biol. Macromol. 209 (2022) 1826–1836, https://doi.org/10.1016/j.ijbiomac.2022.04.156.

[45] N. Lohmann, L. Schirmer, P. Atallah, E. Wandel, R.A. Ferrer, C. Werner, et al., Glycosaminoglycan-based hydrogels capture inflammatory chemokines and rescue defective wound healing in mice, Sci. Transl. Med. 9 (2017), https://doi.org/10.1126/scitranslmed.aai9044.

[46] I.R. Sweeney, M. Miraftab, G. Collyer, A critical review of modern and emerging absorbent dressings used to treat exuding wounds, Int. Wound J. 9 (2012) 601–612, https://doi.org/10.1111/j.1742-481X.2011.00923.x.

[47] X. Tian, H. Jin, J. Sainio, R.H.A. Ras, O. Ikkala, Droplet and fluid gating by biomimetic janus membranes, Adv. Funct. Mater. 24 (2014) 6023–6028, https://doi.org/10.1002/adfm.201400714.

[48] L. Shi, X. Liu, W. Wang, L. Jiang, S. Wang, A self-pumping dressing for draining excessive biofluid around wounds, Adv. Mater. 31 (2019) 1–9, https://doi.org/10.1002/adma.201804187.

[49] A. Sasidharan, L.S. Panchakarla, A.R. Sadanandan, A. Ashokan, P. Chandran, C. M. Girish, et al., Hemocompatibility and macrophage response of pristine and functionalized graphene, Small 8 (2012) 1251–1263, https://doi.org/10.1002/smll.201102393.

[50] S. Cao, G. Xu, Q. Li, S. Zhang, Y. Yang, J. Chen, Double crosslinking chitosan sponge with antibacterial and hemostatic properties for accelerating wound repair, Compos. B Eng. 234 (2022), 109746, https://doi.org/10.1016/j.compositesb.2022.109746.

[51] X. Zhao, B. Guo, H. Wu, Y. Liang, P.X. Ma, Injectable antibacterial conductive nanocomposite cryogels with rapid shape recovery for noncompressible hemorrhage and wound healing, Nat. Commun. 9 (2018), https://doi.org/10.1038/s41467-018-04998-9.

[52] C. Xu, Y. Zhang, K. Xu, J.-J. Nie, B. Yu, S. Li, et al., Multifunctional cationic nanosystems for nucleic acid therapy of thoracic aortic dissection, Nat. Commun. 10 (2019) 3184, https://doi.org/10.1038/s41467-019-11068-1.

[53] Q. Wang, W. Qiu, H. Liu, X. Li, X. Qin, X. Wang, et al., Conductive hydrogel dressings based on cascade reactions with photothermal effect for monitoring and treatment of diabetic wounds, Compos Part B 242 (2022), 110098, https://doi.org/10.1016/j.compositesb.2022.110098.

[54] K.J. Kearney, N. Pechlivani, R. King, C. Tiede, F. Phoenix, R. Cheah, et al., Affimer proteins as a tool to modulate fibrinolysis, stabilize the blood clot, and reduce bleeding complications, Blood 133 (2019) 1233–1244, https://doi.org/10.1182/blood-2018-06-856195.

[55] A. Miszta, A.K. Kopec, A. Pant, L.A. Holle, J.R. Byrnes, D.A. Lawrence, et al., A high-fat diet delays plasmin generation in a thrombomodulin-dependent manner

in mice, Blood 135 (2020) 1704–1717, https://doi.org/10.1182/blood.2019004267.
[56] C. Long, Y. Qing, S. Li, M. Cui, M. Han, K. An, et al., Asymmetric composite wound nanodressing with superhydrophilic/superhydrophobic alternate pattern for reducing blood loss and adhesion, Compos. B Eng. 223 (2021), 109134, https://doi.org/10.1016/j.compositesb.2021.109134.
[57] Q. Fan, R. Ou, X. Hao, Q. Deng, Z. Liu, L. Sun, et al., Water-Induced self-assembly and in situ mineralization within plant phenolic glycol-gel toward ultrastrong and multifunctional thermal insulating aerogels, ACS Nano (2022), https://doi.org/10.1021/acsnano.2c00755.
[58] J. Lyu, Z. Liu, X. Wu, G. Li, D. Fang, X. Zhang, Nanofibrous kevlar aerogel films and their phase-change composites for highly efficient infrared stealth, ACS Nano 13 (2019) 2236–2245, https://doi.org/10.1021/acsnano.8b08913.
[59] S. Mondal, Phase change materials for smart textiles - an overview, Appl. Therm. Eng. 28 (2008) 1536–1550, https://doi.org/10.1016/j.applthermaleng.2007.08.009.
[60] H. Zhang, X. Wang, Synthesis and properties of microencapsulated n-octadecane with polyurea shells containing different soft segments for heat energy storage and thermal regulation, Sol. Energy Mater. Sol. Cells 93 (2009) 1366–1376, https://doi.org/10.1016/j.solmat.2009.02.021.
[61] C. Li, H. Yu, Y. Song, M. Wang, Z. Liu, A n-octadecane/hierarchically porous TiO2 form-stable PCM for thermal energy storage, Renew. Energy 145 (2020) 1465–1473, https://doi.org/10.1016/j.renene.2019.06.070.
[62] Z. Zhang, G. Shi, S. Wang, X. Fang, X. Liu, Thermal energy storage cement mortar containing n-octadecane/expanded graphite composite phase change material, Renew. Energy 50 (2013) 670–675, https://doi.org/10.1016/j.renene.2012.08.024.
[63] J. Yu, L. Yang, X. Liang, T. Dong, H. Qu, M. Rong, et al., Aptamer and PNIPAAm co-conjugated nanoparticles regulate activity of enzyme with different temperature, Talanta 159 (2016) 47–54, https://doi.org/10.1016/j.talanta.2016.05.077.
[64] F.B. Rogers, K.J. Rittenhouse, B.W. Gross, The golden hour in trauma: dogma or medical folklore? Injury 46 (2015) 525–527, https://doi.org/10.1016/j.injury.2014.08.043.
[65] L. Yu, H. Zhang, L. Xiao, J. Fan, T. Li, A bio-inorganic hybrid hemostatic gauze for effective control of fatal emergency hemorrhage in “platinum ten minutes, ACS Appl. Mater. Interfaces (2021), https://doi.org/10.1021/acsami.1c24668.
[66] J. Zhang, F. Zhang, J.-F. Dong, Coagulopathy induced by traumatic brain injury: systemic manifestation of a localized injury, Blood 131 (2018), https://doi.org/10.1182/blood-2017-11-784108, 2001–6.
[67] Y. Sakurai, E.T. Hardy, B. Ahn, R. Tran, M.E. Fay, J.C. Ciciliano, et al., A microengineered vascularized bleeding model that integrates the principal components of hemostasis, Nat. Commun. 9 (2018) 509, https://doi.org/10.1038/s41467-018-02990-x.
[68] R. Troisi, V. Napolitano, V. Spiridonova, I. Russo Krauss, F. Sica, Several structural motifs cooperate in determining the highly effective anti-thrombin activity of NU172 aptamer, Nucleic Acids Res. 46 (2018) 12177–12185, https://doi.org/10.1093/nar/gky990.
[69] K. Göbel, S. Pankratz, C.-M. Asaridou, A.M. Herrmann, S. Bittner, M. Merker, et al., Blood coagulation factor XII drives adaptive immunity during neuroinflammation via CD87-mediated modulation of dendritic cells, Nat. Commun. 7 (2016), 11626, https://doi.org/10.1038/ncomms11626.
[70] X. Sun, Z. Tang, M. Pan, Z. Wang, H. Yang, H. Liu, Chitosan/kaolin composite porous microspheres with high hemostatic efficacy, Carbohydr. Polym. 177 (2017) 135–143, https://doi.org/10.1016/j.carbpol.2017.08.131.
[71] M.R. Di Tullio, S. Homma, Z. Jin, R.L. Sacco, Aortic atherosclerosis, hypercoagulability, and stroke the APRIS (aortic plaque and risk of ischemic stroke) study, J. Am. Coll. Cardiol. 52 (2008) 855–861, https://doi.org/10.1016/j.jacc.2008.04.062.
[72] X. Du, L. Wu, H. Yan, Z. Jiang, S. Li, W. Li, et al., Microchannelled alkylated chitosan sponge to treat noncompressible hemorrhages and facilitate wound healing, Nat. Commun. 12 (2021) 1–16, https://doi.org/10.1038/s41467-021-24972-2.
[73] H. Xu, Q. Zhao, N. Song, Z. Yan, R. Lin, S. Wu, et al., AdipoR1/AdipoR2 dual agonist recovers nonalcoholic steatohepatitis and related fibrosis via endoplasmic reticulum-mitochondria axis, Nat. Commun. 11 (2020) 5807, https://doi.org/10.1038/s41467-020-19668-y.
[74] X. Shi, Y. Cheng, J. Wang, H. Chen, X. Wang, X. Li, et al., 3D printed intelligent scaffold prevents recurrence and distal metastasis of breast cancer, Theranostics 10 (2020) 10652–10664, https://doi.org/10.7150/thno.47933.
[75] H. He, W. Zhou, J. Gao, F. Wang, S. Wang, Y. Fang, et al., Efficient, biosafe and tissue adhesive hemostatic cotton gauze with controlled balance of hydrophilicity and hydrophobicity, Nat. Commun. 13 (2022) 552, https://doi.org/10.1038/s41467-022-28209-8.